Aeroelastic energy harvesting behaviour with combined nonlinear stiffness and nonlinear electromechanical coupling

São Paulo State University

School of Engeenering, Bauru

Ana Carolina Godoy Amaral

July, 2020

Aeroelastic energy harvesting behaviour with combined nonlinear stiffness and nonlinear electromechanical coupling

Ana Carolina Godoy Amaral

A dissertation presented for the degree of Master of Science at the São Paulo State University in a partial fulfillment of the requirements. Supervisor: Prof. Dr. Marcos Silveira

July, 2020

Amaral, Ana Carolina Godoy.
Aeroelastic energy harvesting behaviour with combined nonlinear stiffness and nonlinear electromechanical coupling / Ana Carolina Godoy Amaral, 2020
69 f. : il.

Orientador: Marcos Silveira

Dissertação (Mestrado)–Universidade Estadual Paulista. Faculdade de Engenharia, Bauru, 2020

1. Energy harvesting. 2. Nonlinear stiffness. 3. Nonlinear electromechanical coupling. 4. Flutter. I. Universidade Estadual Paulista. Faculdade de Engenharia. II. Título.

ATA DA DEFESA PÚBLICA DA DISSERTAÇÃO DE MESTRADO DE ANA CAROLINA GODOY AMARAL, DISCENTE DO PROGRAMA DE PÓS-GRADUAÇÃO EM ENGENHARIA MECÂNICA, DA FACULDADE DE ENGENHARIA - CÂMPUS DE BAURU.

Aos 31 dias do mês de julho do ano de 2020, às 09:00 horas, no(a) Via Sistema de videoconferência e outras ferramentas de comunicação a distância, reuniu-se a Comissão Examinadora da Defesa Pública, composta pelos seguintes membros: Prof. Dr. MARCOS SILVEIRA - Orientador(a) do(a) Departamento de Engenharia Mecânica / Faculdade de Engenharia de Bauru - UNESP, Prof. Dr. FABRICIO CESAR LOBATO DE ALMEIDA do(a) Departamento de Engenharia de Biossistemas / Faculdade de Ciências e Engenharia de Tupã - UNESP, Prof. Dr. CARLOS DE MARQUI JUNIOR do(a) Departamento de Engenharia Aeronáutica / Universidade de São Paulo/São Carlos, sob a presidência do primeiro, a fim de proceder a arguição pública da DISSERTAÇÃO DE MESTRADO de ANA CAROLINA GODOY AMARAL, intitulada **AEROELASTIC ENERGY HARVESTING BEHAVIOUR WITH COMBINED NONLINEAR STIFFNESS AND NONLINEAR ELECTROMECHANICAL COUPLING**. Após a exposição, a discente foi arguida oralmente pelos membros da Comissão Examinadora, tendo recebido o conceito final: APROVADA. Nada mais havendo, foi lavrada a presente ata, que após lida e aprovada, foi assinada pelos membros da Comissão Examinadora.

Prof. Dr. MARCOS SILVEIRA

Prof. Dr. FABRICIO CESAR LOBATO DE ALMEIDA P/

Prof. Dr. CARLOS DE MARQUI JUNIOR P/

Aeroelastic energy harvesting behaviour with combined nonlinear stiffness and nonlinear electromechanical coupling

Ana Carolina Godoy Amaral

Keywords: energy harvesting, nonlinear stiffness, nonlinear electromechanical coupling, flutter

Abstract - Energy harvesting is a promising technology to obtain renewable energy, and has attracted much attention, lately. Its objective is to capture the energy present in the environment and transfer it to the various electronic devices in the system. The objective of this work is to study energy harvesting using a piezoelectric transducer applied to an aeronautical structure in flutter condition, with combined nonlinear stiffness and nonlinear electromechanical coupling. The mathematical model for dynamic analysis of a aeroelastic typical section under the described conditions is analysed through numerical simulation. The influence of nonlinear stiffness and nonlinear electromechanical coupling is analysed by quantifying the system's mechanical and electrical power and the system's flutter speed. Flutter speed and mechanical and electrical power as a function of electromechanical coupling are compared for four cases: linear stiffness and linear electromechanical coupling, nonlinear stiffness and linear electromechanical stiffness, linear stiffness and nonlinear electromechanical coupling and nonlinear stiffness and nonlinear electromechanical coupling. Nonlinear stiffness has more influence in flutter speed, while nonlinear electromechanical coupling has more influence on harvested electrical power. Neglecting one nonlinear element characteristic can lead to underestimation of flutter speed and harvested energy, the best result is given by the two nonlinear elements combined. Increasing flutter speed is interesting for aeronautics, as it allows for increased flight speed. And increasing harvested power can extend the applicability of energy harvesting in aeronautical structures and engineering systems in general.

Resposta de energy harvesting aeroelástico com rigidez não linear e acoplamento eletromecânico não linear combinados

Ana Carolina Godoy Amaral

Keywords: energy harvesting, rigidez não linear, acoplamento eletromecânico não linear, flutter

Resumo - Energy harvesting é uma tecnologia promissora para a obtenção de energia renovável, e tem chamado muita atenção, ultimamente. Seu objetivo é extrair a energia presente no ambiente e transferi-la para os diversos dispositivos eletrônicos do sistema. O objetivo deste trabalho é estudar energy harvesting utilizando um transdutor piezoelétrico aplicado a uma estrutura aeronáutica em condição de flutter, com rigidez não linear e acoplamento eletromecânico não linear combinados. O modelo matemático para análise dinâmica da seção aeroelástica típica nas condições descritas é analisado por meio de simulação numérica. A influência da rigidez não linear e do acoplamento eletromecânico não linear é analisada pela quantificação da potência mecânica e elétrica do sistema e da velocidade de flutter do sistema. Velocidade de flutter e potência mecânica e elétrica em função do acoplamento eletromecânico são comparados para quatro casos: rigidez linear e acoplamento eletromecânico linear, rigidez não linear e acoplamento eletromecânico linear, rigidez linear e acoplamento eletromecânico não linear, e rigidez não linear e acoplamento eletromecânico não linear. A rigidez não linear tem mais influência na velocidade de flutter, enquanto o acoplamento eletromecânico não linear tem mais influência na energy harvesting. Negligenciar um elemento não linear pode levar à subestimação da velocidade de flutter e da energy harvesting, o melhor resultado é dado pelos dois elementos não lineares combinados. O aumento da velocidade de flutter é interessante para a aeronáutica, pois permite maior velocidade de voo. E o aumento da energy harvesting pode estender a aplicabilidade da coleta de energia em estruturas aeronáuticas e sistemas de engenharia em geral.

Acknowledgements

I am grateful my family and friends for all of their support. I would like to express my deepest gratitude and respect to my advisor, Marcos Silveira. I am grateful to CAPES (Coordenação de Aperfeiçoamento de Pessoal de Nível Superior) for the financial support (Process Number 88882.432812/2019-01).

Contents

List of Figures

List of Tables

Nomenclature

Designation	Explanation
Latin symbols	
b	semichord of the airfoil
$\tilde{B}$	structural damping matrix
C_p	piezoelectric equivalent capacitante
c	span length
d_α	pitch damping coefficient
d_h	plunge damping coefficient
D_f	difference between the penultimate peak and last peak
D	aerodynamic matrix
E	tolerance
E_1	aerodynamic matrix
E_2	aerodynamic matrix
F	aerodynamic matrix
g	vector with nonlinear terms
h	plunge displacement
I_a	moment of inertia
I	identity matrix
K	nonlinear electromechanical coefficient
k_h	equivalent stiffness coefficient
$\tilde{K}$	structural damping matrix

L	aerodynamic lift
L_h	dimensionless aerodynamic lift
m	airfoil mass
m_n	equivalent mass
m_e	airfoil attachment mass in the springs
M	aerodynamic moment
M_α	dimensionless aerodynamic moment
$\tilde{M}$	structural mass matrix
P	instantaneous power
Q	electrical charge
R_t	load resistance
r_α	radius of gyration
t	time
U	wind speed
v	electrical voltage
x_α	dimensionless chord-wise offset of the elastic axis from the centroid
x_f	distance from the beginning of the airfoil to the torsion center
x_1	augmented aerodynamical state
x_2	augmented aerodynamical state

Greek symbols

α	pitch displacement
β	dimensionless mass ratio
γ	dimensionless frequency ratio
Γ	excitation amplitude
δ	nonlinear stiffness coefficient

ϵ	small parameter
ζ_h	dimensionless plunge damping coefficient
ζ_α	dimensionless pitch damping coefficient
η	dimensionless equivalent capacitance
θ	electromechanical coupling
Θ	strain-dependent coupling coefficient
κ	dimensionless electromechanical coupling
λ	dimensionless load resistance
ρ	fluid density
τ	dimensionless time
Ω	excitation frequency
ω_h	plunge natural frequency
ω_α	pitch natural frequency

Chapter 1

Introduction

The ever increasing need for efficient and environmental-friendly energy sources has propelled the study of some new technologies, such as energy harvesting and its applications in many fields of engineering in the last decade (Safaei et al., 2019; Petrescu et al., 2016; Wei and Jing, 2017; Harb, 2011). For example, the search for sustainability in aeronautics, currently, makes energy harvesting an interesting theme (Wang et al., 2020). This technology has as main objective to capture the energy present in the environment due to the movement of objects, the vibration of structures, or the human movement to direct it to the various electronic devices available, usually to power small and remote electronic devices. One advantage for these electronic devices to be powered by mechanical vibrations is to reduce the need for maintenance, such as battery replacement, which then allows for use in more remote locations.

One important question in applications is how to improve this technology to be able to convert the maximum amount of energy from one given input (Stephen, 2006; Yang et al., 2017), since a common problem is the limited life-time and necessity for periodic recharging or replacement of batteries (Safaei et al., 2019). Tehrani and Elliott (2014) showed that it is possible to increase the energy harvesting dynamic range by introducing nonlinear damping, in this case with a cubic term. The power is measured with several different parameters, so it is perceived that the power captured with the nonlinear damping is greater than that captured with the linear damping, when in resonance, at an excitation below its maximum excitation. Marqui Jr and Marques (2005) created a flexible assembly system, which represents a dynamic system of two degrees of freedom, pitch and plunge, in which a rigid wing encounters classic flutter vibration in a wind tunnel. A mathematical model is proposed to gain insight into system operation, and can later work with flutter suppression, and keep the system stable over a wide range of test speeds. The results shows that it is possible to control complex phenomena such as flutter.

Nonlinear aeroelastic system presents some differences when compared to traditional linear aeroelastic systems. Nonlinear aeroelasticity is the study of the interactions between inertial, elastic and aerodynamic forces in interaction with airspeed and with elements that present nonlinearity that can not be neglected. Concerning flutter speed, Dimitriadis (2017) defines a nonlinear system undergoing LCO (limited cicle oscillations) can be conceptualised as a time-varying linear system undergoing flutter intermittently over each oscillation cycle. The term 'flutter speed' is more commonly used for linear aeroelastic, however, it can, also, be applied in nonlinear aeroelasticity. Sousa et al. (2017) employs a Synchronized Switch Damping on Inductor (SSDI) technique, which is capable of dealing with the nonlinear characteristics of the electrical domain of the problem, and the use of shape memory alloys (SMA) as an alternative to conventional actuators. The nonlinearity applied to the system by the SMA and SSDI together results in better aeroelastic behaviour, so stable LCOs of acceptable amplitudes are obtained for a range of velocities 25 % higher than in the linear flutter speed of the system. Wang et al. (2017) shows nonlinear harvesters can maximize the power output from human motions. Triplett and Quinn (2009) indicate that the amount of the energy harvested can be increased, when nonlinear stiffness and nonlinear electromechanical coupling is included.

1.1 Motivation

At the last decade, energy harvesting has been investigated as a responsible manner of producing and consuming energy, with aeronautics being an area of application. Energy harvesting is responsible for scavenging power from ambient vibration and transfer it to electrical devices, however, the applicability of energy harvesting needs to be improved. So, the motivation of the project is to increase the amount of energy harvested including combined nonlinear stiffness and nonlinear electromechanical coupling in aeroelastic typical section, to make this technology more interesting for society.

1.2 Objectives

The objective of this work is to study the dynamic behaviour of an energy harvesting system using a piezoelectric transducer applied to an aeronautical structure in flutter condition, with combined nonlinear stiffness and nonlinear electromechanical coupling. This main objective is divided into three parts:

- Obtain a simplified mathematical model of an aeroelastic typical section, with two mechanical degrees of freedom related to plunge and pitch, and one electrical degree of freedom.

- Identify the influence of nonlinear stiffness on the energy harvesting and on the flutter speed.

- Identify the influence of nonlinear electromechanical coupling on the energy harvesting and on the flutter speed.

1.3 Literature review

The literature review shows some relevant aspects for understanding the main features which this work is based on. The definition of aeroelasticity and the phenomenon of flutter is presented, as well as energy harvesting and its types of application. It approaches some authors and their respective studies referring to aeroelastic systems and advantages of applying nonlinear elements in the system.

1.3.1 Aeroelasticity

Aeroelasticity is a science whose objectives of study are elastic, inertial and aerodynamic forces in interaction with air (Bisplinghoff et al., 2013). Energy harvesting can be applied in aeroelasticity to generate renewable energy. Many applications have been proposed, such as low-power electricity generation in various applications ranging from aircraft and rotorcraft to civil structures in high wind areas (Marqui Jr et al., 2018; Marqui Jr and Erturk, 2013). Figure 1.1 shows the triangle of forces, also called Collar triangle (Collar, 1946), to understand and visualise this study area.

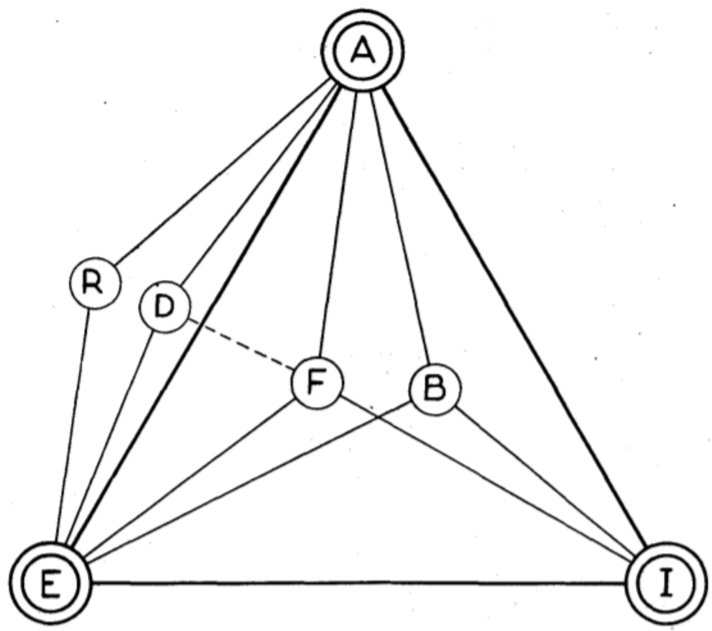

Figure 1.1: Collar triangle. A is aerodynamic forces, E is elastic forces, I is the inertia forces, F is flutter, B is buffeting, D is divergence and R is reversal control. Source: Collar (1946).

The interaction between the elastic and aerodynamic forces stands for static aeroelasticity, which encompasses the phenomenon of divergence and reversal control (Yoon et al., 2012). However, when the inertia force is included, we have the dynamic aeroelasticity, which encompasses the phenomenon of buffeting and flutter. These are the classical phenomena of aeroleasticity, they correspond to a dynamical instability of the system. Flutter and divergence are part of the stability problems, while buffeting and reversal contral are system response problems. In this work, flutter is analysed, which is a very important topic in aeroelasticity.

Flutter phenomenon occurs when an aircraft component presents a divergent oscillatory self-sustained behaviour at a given speed. It is an undesirable phenomenon in aircraft because it can cause structural damage due to the aeroelastic instability. As explaining earlier, Dimitriadis (2017) defines a nonlinear system undergoing LCO can be conceptualised as a time-varying linear system undergoing flutter intermittently over each oscillation cycle. For nonlinear aeroelastic system, the nomenclature for the speed, in which this phenomenon happens, is critical velocity, or, like in linear system, flutter speed. For this work, the term 'flutter speed' is used for linear and, also, nonlinear aeroelastic systems.

However, this oscillatory movement, caused by the flutter phenomenon, is an interesting source of research and study for energy harvesting technology. As energy is transferred from the mechanical oscillations to the electrical domain, energy harvesting can be seen as a means to attenuate, control or retard typical aeroelastic phenomena, such as flutter (Jonsson et al., 2019; Tsushima and Su, 2017), galloping (Jung and Lee, 2011; Abdelkefi et al., 2012a), and VIV (vortex induced vibrations) (Zhang et al., 2017a). For example, flutter speed, or the speed at which potentially dangerous self-sustained limit cycle oscillations occur, can be increased by using a piezoelectric harvester. However, in low power applications this change in flutter speed can be small, and this can be seen as a secondary benefit. Summarizing, if flutter speed could be increased, energy harvesting can be an interesting theme for aeronautics. The other benefit from energy harvesting is extracting electrical power from flutter vibrations and direct it to electronic aircraft devices.

1.3.2 Energy harvesting

Energy harvesters are designed to scavenge power from ambient vibration and transfer it to electrical devices (Bibo and Daqaq, 2013; Harb, 2011). It is a promising technology to produce sustainable power sources and replacing fossils fuels. There are many energy harvesting applications: including sensors in smart structures, (Gatti et al., 2016; Roundy and Wright, 2004; Amirtharajah and Chandrakasan, 1998), allowing the use of wireless sensors in remote locations with minimal maintenance, such as structures under fluid flow excitations (Tang et al., 2009; Bibo and Daqaq, 2013; Erturk et al., 2010; Jonsson et al., 2019), extracting energy from self-sustained fluid induced oscillations, regenerative suspension in hybrid or electric vehicles (Zhang et al., 2017b; Zuo et al., 2010), reusing energy otherwise dissipated in viscous dampers thus increasing range; any devices in which replacing batteries is undesirable, reducing chemical waste from discarded batteries.

The piezoelectric energy harvesting is used in this work, due to its scope and for have previously been successful in linear systems (Marqui Jr and Erturk, 2013; Caliò et al., 2014). Certain materials with crystalline structures such as quartz, can generate electric energy when an external mechanical force is applied. So piezoelectric harvesting, when subjected to pressure, generates a electric field, that is transforming in electric power to be used in electronic devices and wireless sensor nodes. Figure 1.2 shows an piezoelectric membrane transducer used to investigate the electric energy harvesting from a mechanical vibration (Ericka et al., 2005).

It is important to take the maximum output power to make this technology more viable. The output power from piezoelectric devices is typically restricted to a few milliWatts. One way to maximize the output power from energy harvesting is to choose the most applicable piezoelectric, for each case (Kang et al., 2016). But the perfor-

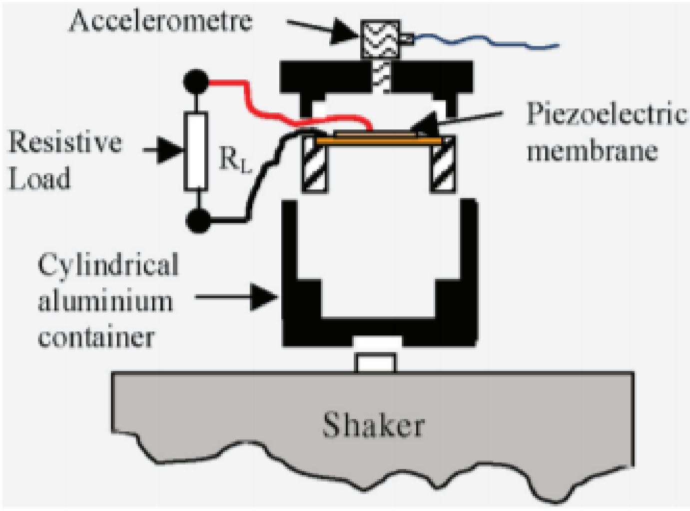

Figure 1.2: Energy harvesting from vibration using a piezoelectric membrane. Source: Ericka et al. (2005).

mance of energy harvesters is still a question. The study of Yang et al. (2017) discuss efficiency work from a piezoelectric energy harvester, in which efficiency is mainly related to the electromechanical coupling effect, damping effect, excitation frequency and electrical load. So, each piezoelectric energy harvesting has its own performance due to parameters, size, weight and material.

The growing interest in green energy by aeronautic, due to climate changing and global warming, makes energy harvesting an interesting choice to help decrease the carbon emissions by aircraft in general (Tsai et al., 2014). Figure 1.3 shows the model of an aeroelastic typical section with piezoelectric transducer at plunge degree of freedom. This approach allows to extract energy from mechanical vibration caused by flutter and transfer it to electronic devices present in the aerolastic system.

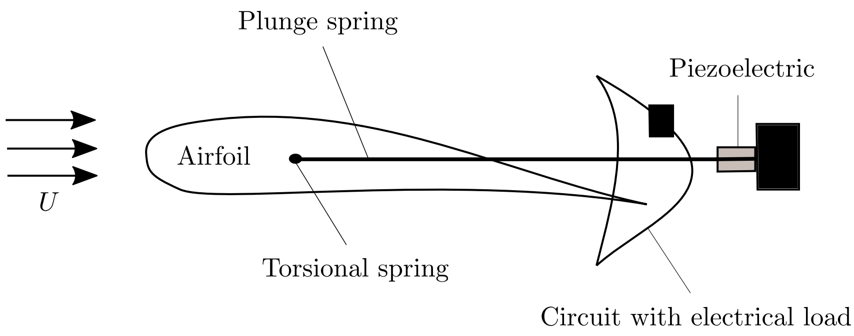

Figure 1.3: Piezoelectric transducer applied to an aeroelastic typical section.

1.3.3 Nonlinear stiffness and nonlinear electromechanical coupling

Nonlinear aspects of energy harvesting have been extensively investigated for two main reasons. One reason is to improve the accuracy of the mathematical models of systems that inherently present nonlinear constitutive relationships due to material or present geometrical nonlinear behaviour due to large displacements (Daqaq et al., 2014). The other reason is to intentionally introduce nonlinear behaviour to the system in order to improve the harvesting performance, which usually involves nonlinear stiffness or damping resulting in larger energy conversion in a broader frequency range (Tehrani and Elliott, 2014; Erturk et al., 2009).

Specifically in aeroelastic energy harvesting, some of the structural nonlinear aspects studied includes freeplay in joints and actuators (Sousa et al., 2011; Tang and Dowell, 2006) and nonlinear stiffness components related to plunge or pitch motion (Abdelkefi et al., 2012b; Erturk et al., 2010). Besides structural nonlinear aspects, electrical nonlinear aspects can have large influence on the aeroelastic harvesting device. The linear models of piezoelectric cantilevers are more commonly used, but with increasing excitation amplitude nonlinear effects are needed to be able to demonstrate the behaviour for hight amplitudes (Goldschmidtboeing et al., 2011). A linear analysis of piezoeletric power harvester is not able to describe the response behaviour of the system without nonlinear electroelasticity, when in resonance (Hu et al., 2006). The nonlinearity of piezoelctric materials are inherent, and it has more than one type. The work of Leadenham and Erturk (2015) develops one unified nonlinear electroelastic dynamics of a bimorph piezoelectric cantilever for energy harvesting, his model has an excellent agreement with experimental tests.

Piezoelectric macro-fiber composite cantilevers, used with interdigitated electrodes for resonant actuation and in energy harvesting, has more than one type of nonlinearity inherent to the system, like piezoelectric softening, geometric hardening, and inertial softening, so linear model can not describe accurately the dynamical behaviour of this type of system (Tan et al., 2018a,b). The presence of nonlinear relationship between strain and electric field can lead to larger voltage generated by the harvester than what is predicted by a linear model (DuToit and Wardle, 2007; Crawley and Anderson, 1990).

Figure 1.4 shows mechanical component of the energy harvesting system used by Triplett and Quinn (2009) to compare the use of nonlinear stiffness and nonlinear electromechanical coupling with the typical section with linear stiffness and linear electromechanical coupling, by quantifying flutter speed, mechanical and electrical power.

The dynamical dimensionless equations of figure 1.4 are reproduced here:

$$
\begin{aligned}
h'' + h &= \epsilon(-\zeta_h h' - \delta h^3 + \kappa(1 + K|h|)v + \Gamma \sin(\Omega\tau)) \\
v' &= (\kappa(1 + K|h|)h - v)/\rho_n; \qquad (1.1)
\end{aligned}
$$

in which h is the dimensionless plunge displacement, ζ_h is the dimensionless plunge damping coefficient, δ is the nonlinear stiffness coefficient, κ is the dimensionless linear electromechanical coupling, K is the nonlinear electromechanical coefficient, ϵ is a smal parameter, v is the dimensionless electrical voltage, Γ is the excitation amplitude, Ω is the excitation frequency, τ is the dimensionless time, $\rho_n = R_t C_p \sqrt{k_h/m_n}$, R_t is the load resistance, C_p is the equivalent capacitance, k_h is the equivalent stiffness, m_n is the

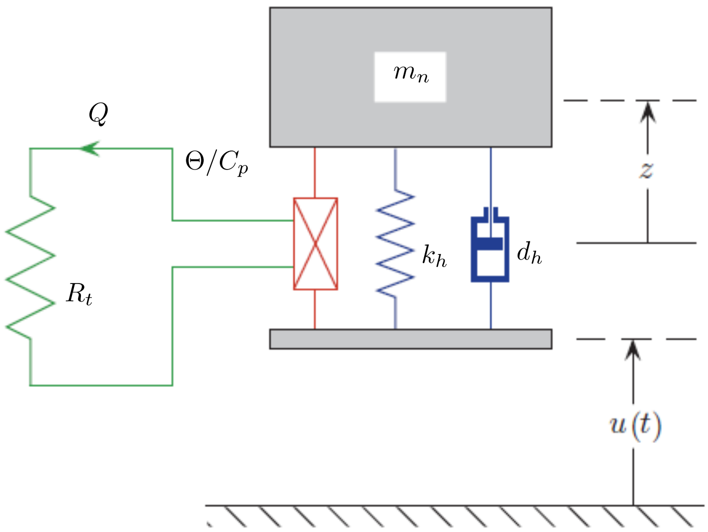

Figure 1.4: Vibration-based energy harvesting, in which m_n is the equivalent mass, k_h is the equivalent stiffness coefficient, d_h is the plunge damping coefficient, $u(t)$ is the motion of the base, $z(t)$ is the relative displacement of the attachment, Q is the electrical charge, Θ is the strain-dependent coupling coefficient, C_p is the piezoelectric equivalent capacitance, R_t is the load resistance. Source: Triplett and Quinn (2009).

equivalent mass, and $'$ denotes differentiation over dimensionless time (τ).

To illustrate the effect of nonlinear electromechanical coupling, some results by Triplett and Quinn (2009) are shown. The time history and the average power as a function of frequency of the aeroelastic section, represented by Eq. (1.1), is shown. The following parameters were adopted: $\Gamma = 2$, $\epsilon = 0.1$, $\zeta_h = 0.25$, $\delta = 0$, $\rho_n = 1$, $\kappa = 1$, $K = 1$, $\Omega = 1$ e $\tau = 2\pi$. The initial conditions used in all simulations were: $h = 0$, $h' = 0$ and $v = 0$. Figures 1.5 and 1.6 shows displacement and power as a function of time and frequency.

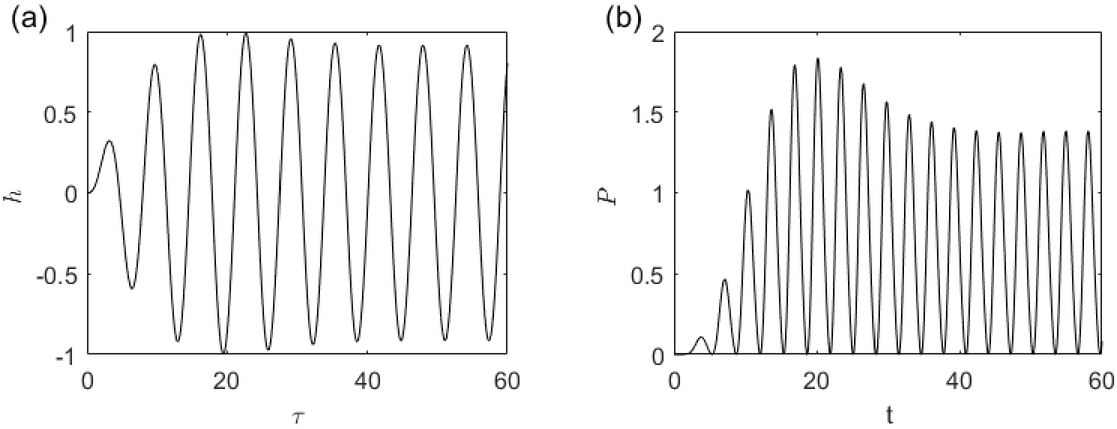

Figure 1.5: (a) Displacement in function of time, (b) Power in function of time.

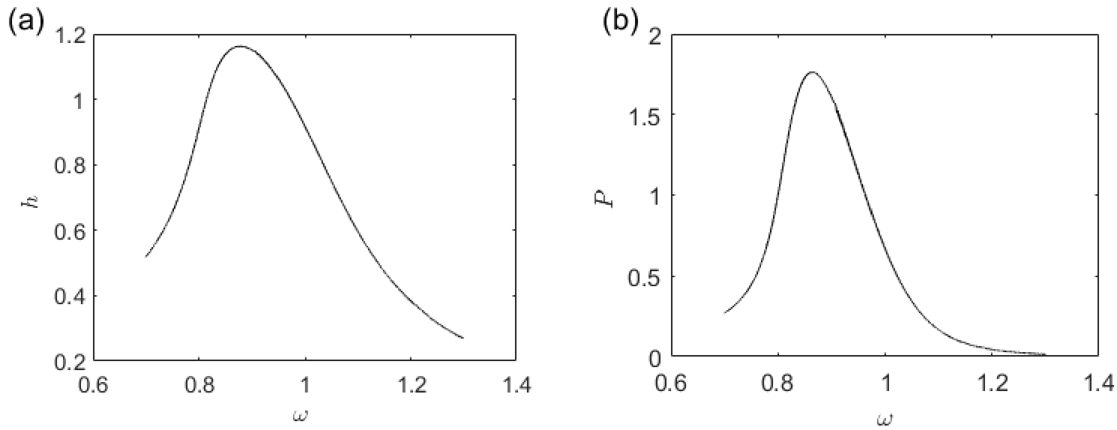

Figure 1.6: (a) Displacement in function of frequency, (b) Power in function of frequency.

Figure 1.7 shows the average power as a function of frequency, varying κ, using linear electromechanical coupling ($K = 0$) and using (a) linear stiffness and (b) nonlinear stiffness. One of the largest output powers is given by $\kappa = 1.0$, witch has the highest peak, so this value of κ is used in subsequent analyses.

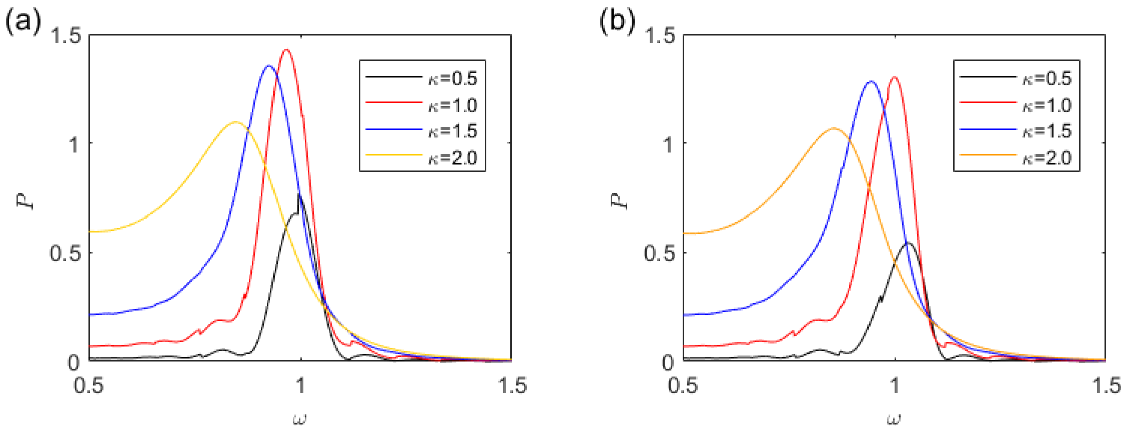

Figure 1.7: (a) Average power in function of frequency with linear stiffness, (b) Average power in function of frequency with nonlinear stiffness.

Figure 1.8 shows the average power as a function of frequency varying K, using nonlinear stiffness. The maximum power harvesting is obtained for $K = 0.5$, so this value of K is used in subsequent analyses.

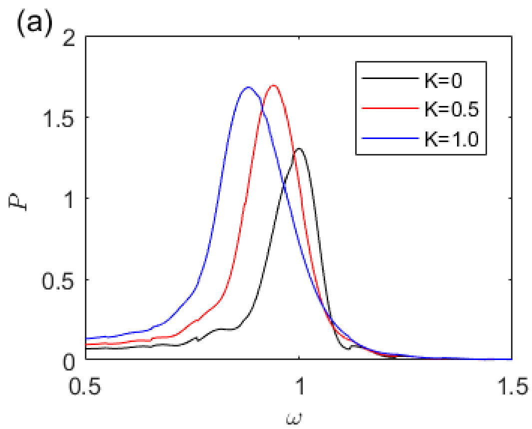

Figure 1.8: Power in function of frequency with nonlinear stiffness.

Figure 1.9 shows average power in function of frequency for $\kappa = 0.5$, $\kappa = 1.0$ and $\kappa = 2.0$, all in four cases: linear stiffness and linear electromechanical coupling, nonlinear stiffness and linear electromechanical coupling, linear stiffness and nonlinear electromechanical coupling and nonlinear stiffness and nonlinear electromechanical coupling. The results indicates that the application of nonlinear electromechanical coupling increases the average power and the application of nonlinear stiffness shifts the peak to the right. It can be concluded that it is interesting for the project to study the system using nonlinear electromechanical coupling and nonlinear stiffness, because the use of nonlinear electromechanical coupling can increase the energy harvesting, besides that the both nonlinear elements combined can produce interesting results.

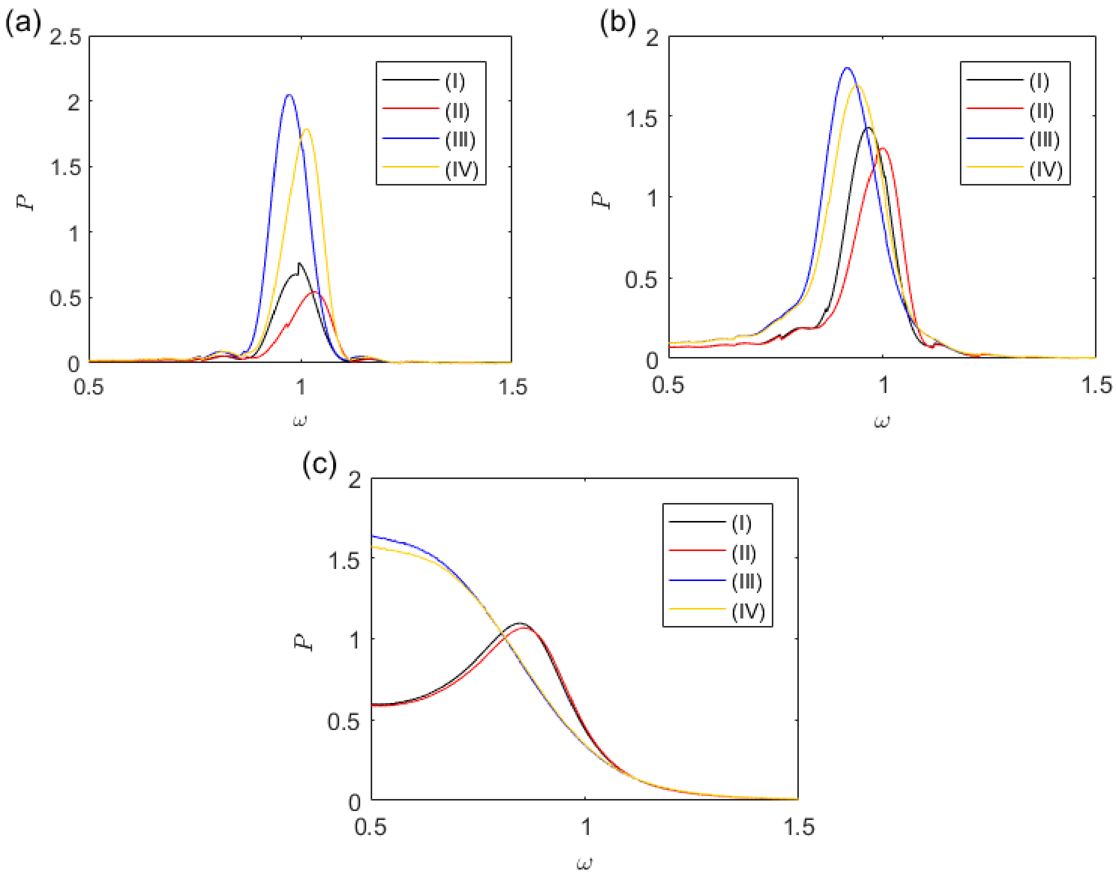

Figure 1.9: Average power in function of frequency (a) for $\kappa = 0.5$, (b) for $\kappa = 1.0$ and (c) for $\kappa = 2.0$. (I) linear stiffness and linear electromechanical coupling, (II) nonlinear stiffness and linear electromechanical coupling, (III) linear stiffness and nonlinear electromechanical coupling, and (IV) nonlinear stiffness and nonlinear electromechanical coupling.

Chapter 2

Mathematical models

In this chapter, the model and the dynamical equations of the aeroelastic typical section are described. Also, the mathematical model for aerodynamic loads is presented. At the end, the methodology that is used in the project is described.

2.1 Aeroelastic typical section

Figure 2.1 shows the model of the aeroelastic typical section of a system with three degrees of freedom: two mechanical degrees of freedom, plunge (h) and pitch (α), and one electrical degree of freedom, voltage (v). The piezoelectric coupling is associated to plunge.

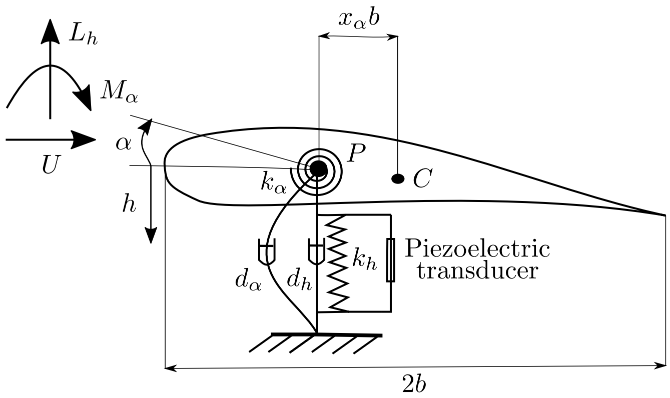

Figure 2.1: Aeroelastic typical section. P is the elastic axis, C is the aerodynamic center, $x_\alpha b$ is the distance between P and C, b is the semichord, h and α are the plunge and pitch displacements, d_α and d_h are the plunge and pitch damping coefficients, k_α and k_h are the plunge and pitch stiffness coefficients, U is the wind velocity, M_α is the dimensionless aerodynamic moment, L_h is the dimensionless aerodynamic lift.

2.1.1 Mathematical model of aeroelastic typical section

The dynamical equations, based on Marqui Jr and Erturk (2013), of the system presented in figure 2.1, applying the nonlinear stiffness of the cubic type associated to plunge movement and nonlinear electromechanical coupling, in dimensionless form, are given by:

$$\begin{aligned} \beta h'' + x_\alpha \alpha'' + \zeta_h h' + h + \delta h^3 - \kappa(K|h'| + 1)v &= -L_h \\ x_\alpha h'' + r_\alpha^2 \alpha'' + \zeta_\alpha \alpha' + \gamma^2 r_\alpha^2 \alpha &= M_\alpha \\ \eta v' + \frac{v}{\lambda} + \kappa(K|h'| + 1)h' &= 0 \end{aligned} \tag{2.1}$$

in which h and α are the dimensionless plunge and pitch displacements, β is the dimensionless mass ratio, ζ_h and ζ_α are the dimensionless plunge and pitch damping ratios, x_α is the dimensionless chord-wise offset of the elastic axis from the centroid, r_α is the dimensionless radius of gyration, γ is the dimensionless frequency ratio, M_α is the dimensionless aerodynamic moment, L_h is the dimensionless aerodynamic lift, κ is the dimensionless electromechanical coupling, λ is the dimensionless load resistance, v is the dimensionless voltage electrical, η is the dimensionless equivalent capacitance, δ is the dimensionless nonlinear stiffness coefficient, K is the dimensionless nonlinear electromechanical coupling coefficient, and $'$ denotes differentiation over dimensionless time (τ).

The dimensionless terms follows the definitions used by Marqui Jr and Erturk (2013), and are reproduced as follows:

$$
\begin{aligned}
&h = \frac{\overline{h}}{b} \qquad &&\beta = \frac{m + m_e}{m} \qquad &&\zeta_h = \frac{d_h}{m\omega_h} \qquad &&\zeta_\alpha = \frac{d_\alpha}{mb^2\omega_h} \qquad &&r_\alpha = \frac{\overline{r}_\alpha}{b} \\
&\gamma = \frac{\omega_\alpha}{\omega_h} \qquad &&v = \frac{\overline{v}}{v^*} \qquad &&\kappa = \frac{\theta v^*}{cmb\omega_h^2} \qquad &&\eta = \frac{C_p v^{*2}}{mb^2c\omega_h^2} \qquad &&\lambda = \frac{R_l mb^2c\omega_h^3}{v^{*2}} \\
&L_h = \frac{L}{mb\omega_h^2} \qquad &&M_\alpha = \frac{M}{mb^2\omega_h^2} \qquad &&U = \frac{\overline{U}}{\omega_h b} \qquad &&\tau = \omega_h t
\end{aligned}
\tag{2.2}
$$

in which m is the typical section mass, m_e is the attachment mass, bx_α is the offset from the elastic axis to the centroid, $\overline{h}$ is the plunge displacement, d_α and d_h are the plunge and pitch damping coefficients, $\overline{r}_\alpha$ radius of gyration, c is the span length, ω_h and ω_α are the uncoupled plunge and pitch natural frequencies, $\overline{v}$ is the electrical voltage, $v^* = 1V$ is the reference voltage for normalisation, R_t is the load resistance, C_p is the piezoelectrical equivalent capacitance, θ is the piezoelectrical coupling, L is the aerodynamic lift, M is the aerodynamic moment, $\overline{U}$ is the wind speed, and t is the time.

2.2 Mathematical models of aerodynamical loads

In this project two models of aerodynamical loads are used: the model of Dimitriadis (2017) and the model of Edwards (1979).

Dimitriadis (2017) presents a mathematical model for the aerodynamic loads, lift (L) and moment (M), for a quasi-steady aerodynamic system in a incompressible flow.

The expressions are reproduced here:

$$
\begin{aligned}
L &= \rho\pi b^2\left(\ddot{\overline{h}} - \left(x_f - \frac{c}{2}\right)\ddot{\alpha}\right) + \rho\pi b^2\overline{U}\dot{\alpha} + \rho\overline{U}^2 c\pi\left(\alpha + \frac{\dot{\overline{h}}}{\overline{\overline{U}}} + \left(\frac{3}{4}c - x_f\right)\frac{\dot{\alpha}}{\overline{\overline{U}}}\right)\\
M &= \rho\pi b^2\left(x_f - \frac{c}{2}\right)\left(\ddot{\overline{h}} - \left(x_f - \frac{c}{2}\right)\ddot{\alpha}\right) - \frac{\rho\pi b^4}{8}\ddot{\alpha} - \left(\frac{3}{4}c - x_f\right)\rho\pi b^2\overline{U}\dot{\alpha}\\
&\quad + \rho\overline{U}^2 e c^2\pi\left(\alpha + \frac{\dot{\overline{h}}}{\overline{\overline{U}}} + \left(\frac{3}{4}c - x_f\right)\frac{\dot{\alpha}}{\overline{\overline{U}}}\right) - \frac{1}{16}\rho\overline{U}c^3\pi\dot{\alpha}
\end{aligned}
\tag{2.3}
$$

in which ρ is the density, b is the semichord of the airfoil, x_f is the distance from the beginning of the aerofoil to the neutral line, and $e = x_f/c - 1/4$. Note that Eq. (2.3) is not in the dimensionless form.

Another way to represent lift (L) and moment (M) from Eq.(2.3) is in the matrix form proposed by Edwards (1979) for an unsteady aerodynamics in incompressible flow. In this formulation, the state variables are h, α, h', α', x_1, x_2, v with $x_a = [x_1 \quad x_2]^t$ being the augmented aerodynamical states. Also, electromechanical coupling must be included in the matrix formulation (Marqui Jr and Erturk, 2013). The dynamical equations of this model including nonlinear elements, in the matrix form, are:

$$
\begin{bmatrix} I & 0 & 0 & 0\\ 0 & \tilde{M} & 0 & 0\\ 0 & 0 & I & 0\\ 0 & 0 & 0 & \eta \end{bmatrix}
\begin{bmatrix} x'\\ x''\\ x_a'\\ \overline{v}' \end{bmatrix}
=
\begin{bmatrix} 0 & I & 0 & 0\\ -\tilde{K} & -\tilde{B} & D & \theta_1\\ E_1 & E_2 & F & 0\\ 0 & -\theta_2 & 0 & -\frac{1}{\lambda} \end{bmatrix}
\begin{bmatrix} x\\ x'\\ x_a\\ \overline{v} \end{bmatrix}
+ g(x, x', x_a, v)
\tag{2.4}
$$

in which $\theta_1 = [0 \quad \kappa]^t$, $\theta_2 = [0 \quad \kappa]$, $x = [\alpha \quad h]^t$, $x_a = [x_1 \quad x_2]^t$, I is the 2x2 identity matrix, $\tilde{M}$, $\tilde{B}$, $\tilde{K}$ are calculated through the respective structural mass, damping and stiffness matrices. $\tilde{M}$, $\tilde{B}$, $\tilde{K}$ and the aerodynamic matrices $\mathbf{D}$, $\mathbf{E_1}$, $\mathbf{E_2}$, $\mathbf{F}$ can be found in Edwards (1979) and $g(x, x', x_a, v)$ is the vector with nonlinear terms.

2.3 Methodology

In this section the methodology of the project is presented by showing how flutter speed, mechanical and electrical power are calculated and compared.

2.3.1 Proposed cases

There are six cases that are evaluated in this work, to study the influence of nonlinear terms:

- Case I: Aeroelastic typical section, with linear stiffness ($\delta = 0$), and with linear electromechanical coupling ($K = 0$).
- Case II: Aeroelastic typical section, with nonlinear stiffness ($\delta = 10$), and with linear electromechanical coupling ($K = 0$).
- Case III: Aeroelastic typical section, with linear stiffness ($\delta = 0$), and with nonlinear electromechanical coupling ($K = 2$).
- Case IV: Aeroelastic typical section, with nonlinear stiffness ($\delta = 10$), and with nonlinear electromechanical coupling ($K = 2$).
- Case V: Aeroelastic typical section, without piezoelectric coupling, with only two mechanical DOFS, with linear stiffness ($\delta = 0$).
- Case VI: Aeroelastic typical section, without piezoelectric coupling, with only two mechanical DOFS, with nonlinear stiffness ($\delta = 10$).

Case I is the linear case, and taken as the baseline for the comparisons. Cases II and III are used to analyse the influence of each nonlinear term independently. Case IV is used to show the combined effect of both nonlinear terms. The flutter speed (U^*) and average power per cycle at flutter speed (P_h^* , P_α^*, P_e^*) are quantified in each case. Cases V and VI consider the system without piezoelectric coupling.

2.3.2 Calculating flutter speed

At this work, optimisation is used to find the flutter speed, because it is needed to quantify flutter speed and average power, when flutter phenomena occurs for each case.

The flutter speed is determined by two different ways. For the linear system (cases I and V), the flutter speed is calculated through analytical stability analysis of the equilibrium point of equations 2.1, such that flutter occurs when at least one eigenvalue has positive real part. For the nonlinear system, the response of the system is calculated through numerical simulation, using a 4th order Runge-Kutta method. The flutter speed was determined with an optimisation procedure based on the interval halving method (or bissection method). In the this method, one-half of the current interval of uncertainty is discarded in every stage, until the right solution is found, for the middle point of the final interval (Rao, 2009).

From a initial guess for the interval, which is taken based on the flutter speed of the linear system, and with the other parameters fixed, the optimisation procedure seeks to minimise the difference between consecutive peaks of the response in time. If the difference is zero, this gives the condition of self-sustained oscillation. Therefore, the objective function is given by:

$$f(U) = |D_f| - E \tag{2.5}$$

in which D_f is the difference between the penultimate amplitude peak and last amplitude peak, and E is a tolerance. Equation (2.5) allows the reasoning that in order for flutter to happen, the distance between the peaks must be 0. Since the equations are solved numerically, a tolerance must be considered.

2.3.3 Calculating instantaneous power

In order to analyse the influence of nonlinear stiffness and nonlinear electromechanical coupling, the average power per cycle is calculated for the mechanical and electrical domains. The instantaneous power dissipated by the mechanical system related to plunge and pitch and the instantaneous electrical power are given by:

$$\overline{P_h} = \zeta_h h'^2 \qquad \overline{P_\alpha} = \zeta_\alpha \alpha'^2 \qquad \overline{P_e} = v^2/\lambda \tag{2.6}$$

with the instantaneous power calculated, it is possible to calculate the average power per cycle, P_h, P_α and P_e (Stephen, 2006). Average power per cycle at flutter speed is represented by P_h^* , P_α^*, P_e^*.

Chapter 3

System behaviour as function of nonlinear terms

In this chapter, the dynamical behaviour of the aeroelastic section described in the previous chapter is presented. The behaviour with the two models of aerodynamical loads, Edwards and Dimitriadis, are compared. The variation of flutter speed as a function of the nonlinear terms, and the displacement as a function of time is discussed to evaluate the effects of nonlinear terms. Mechanical and electrical power as a function of the wind speed are also analysed.

3.1 Comparison of models of aerodynamical loads

In this section, the behaviour of the aeroelastic section in case I, using the models of aerodynamical loads from Edwards (1979) and from Dimitriadis (2017) are compared considering linear stiffness. Although the Edwards' model is more commonly used, the Dimitriadis' model is more easily adaptable for nonlinear analysis, as the former is given in matrix form and uses augmented variables (x_a). For both models, an analytical simulation and a numerical simulation was performed, as numerical simulation is used in the following sections when considering nonlinear stiffness.

The values of parameters used here are given in Table 3.1, base on values from (Marqui Jr and Erturk, 2013):

Table 3.1: Nominal values of parameters

Parameters	Edwards	Dimitriadis
β	2.5940	2.5940
$\overline{r}_\alpha$	0.5467	0.5467
γ	0.5090	0.5090
ζ_h	0.0535	0.0535
ζ_α	0.1102	0.1102
x_α	0.25	0.25
ρ	1.2754kg/m^3	1.2754kg/m^3
b	0.76 m	0.76 m
κ	5.9×10^{-6}	5.9×10^{-6}
η	3.66×10^{-9}	3.66×10^{-9}
λ	0.48×10^{9}	0.48×10^{9}
x_f	$b - x_\alpha b$	$b - x_\alpha b$
c	$b/2$	$b/2$
m	92.53 kg	92.53 kg
ω_h	50 rad/s	50 rad/s
a	-0.4	–
μ	40	–

The initial conditions used are given in Table 3.1.

Table 3.2: Initial conditions

Initial conditions adopted	Edwards	Dimitriadis
$\overline{h}$	0.1	0.1
α	0.1	0.1
$\overline{h}'$	0	0
α'	0	0
$\overline{v}$	0	0
x_1	0.1	–
x_2	0.1	–

Figure 3.1 shows the variation of the flutter speed (U^*) as a function of the electromechanical coupling, for case I, for the two models of the aerodynamic loads, calculated analytically (a) and numerically (b). The electromechanical coupling (κ) varies from 2×10^{-6} to 10×10^{-6}.

The largest difference between the aerodynamical models happens at lower values of

κ. For example $\kappa = 2 \times 10^{-6}$, the difference is 0.038, for numerical solution and 0.037, for analytical solution. This result indicates that both models have similar results under these conditions. Therefore, as nonlinear analysis is the purpose of this project, the Dimitriadis' model is used in all subsequent analyses.

The largest difference of U^* between the analytical and numerical solutions for the aerodynamic model from Dimitriadis is 2×10^{-3}, while for the aerodynamic model from Edwards is 3×10^{-3}. This shows that the numerical solution is a good approximation, and is used in the analyses considering nonlinear stiffness.

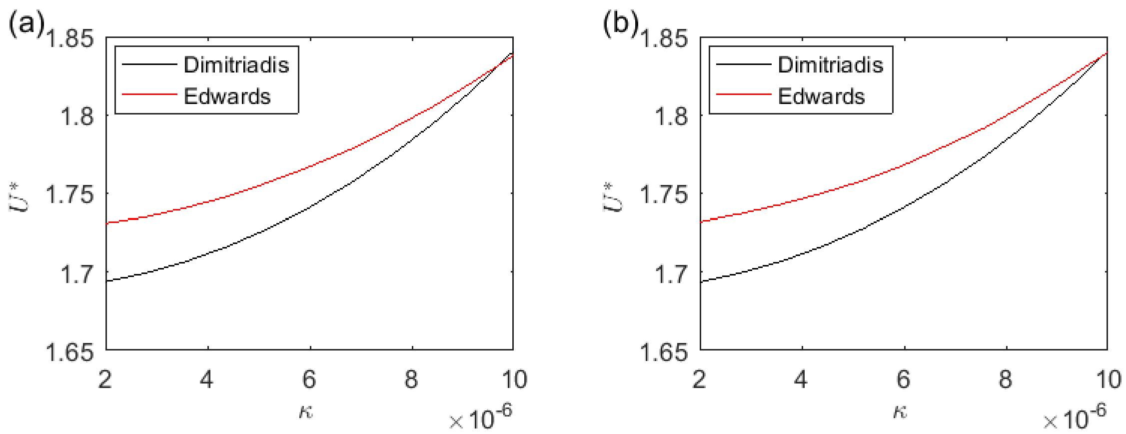

Figure 3.1: Flutter speed as a function of the electromechanical coupling for aerodynamic models from Dimitriadis (2017) and from Edwards (1979): (a) analytical solution by calculating the eigenvalues; (b) numerical solution using the fourth order Runge-Kutta method.

Figure 3.2 shows variation of the real and imaginary parts of the system eigenvalues with air speed, for case I and Dimitriadis' model, using nominal parameters. The real eigenvalues is equivalent to the damping factor in function of airspeed, which is shown in Fig. 3.2(a). The imaginary eigenvalues, however, is the frequency, which is shown in Fig. 3.2(b). At least one of the real eigenvalues becomes zero at the flutter speed (U^*), this can be seen at the red point. The value of U^* is 1.739 equivalent to figure 3.1.

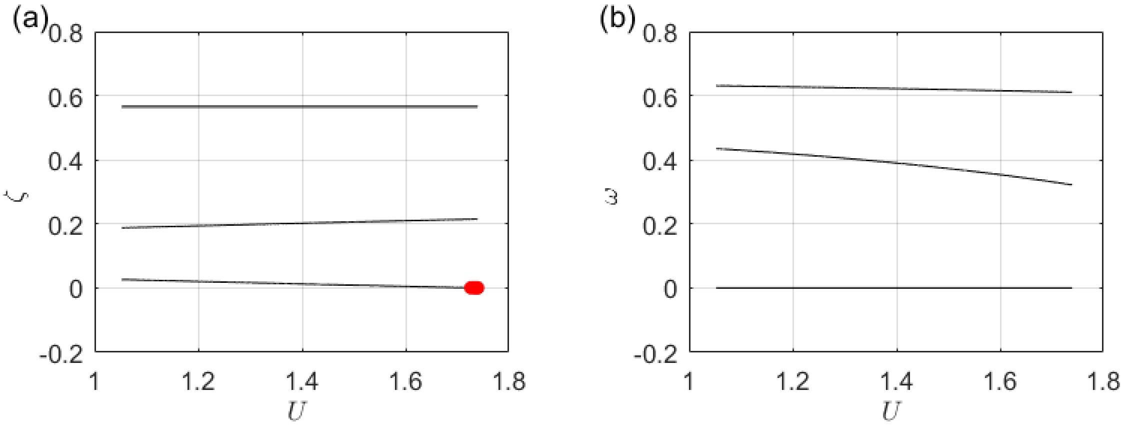

Figure 3.2: (a) Damping ratio as a function of air speed; (b) Frequency ratio as a function of air speed;

3.2 Flutter speed as a function of nonlinear terms

Exceptionally, in this section, the value of K is 10. Figure 3.3 shows that U^* increases by the same amount in this interval with both δ and K, and it has almost linear behaviour with respect to the former. Also, P_h^* increases with both nonlinear terms, while P_α^* increases with δ but decreases with K. P_e^* is very insensitive to δ, although very sensitive to K.

In figure 3.4 a, it can be observed that changes in δ and K incur changes in amplitude and frequency. As the response of the autonomous system given by equations 2.2 at flutter speed is a limit-cycle, a Poincaré section Σ was used on the state space [h, h', α, α', v] in order to determine the period of oscillations. Such section is defined by:

$$\Sigma = \left\{(h, h', \alpha, \alpha', v) \in \mathcal{R}^1 \times \mathcal{R}^1 \times \mathcal{R}^1 \times \mathcal{R}^1 \times \mathcal{R}^1 \,|\, h = 0\right\} \tag{3.1}$$

With this procedure, the period (T) for cases I–IV were found to be $T_I = 10.29$, $T_{II} = 9.75$, $T_{III} = 10.32$ and $T_{IV} = 9.77$, indicating that, as $\delta > 0$ results in hardening stiffness characteristic, in which overal stiffness is increased, frequency is also increased. However, $K > 0$ decreases the frequency, although the system is less sensitive to this parameter. This behaviour is illustrated in figure 3.4 b–c.

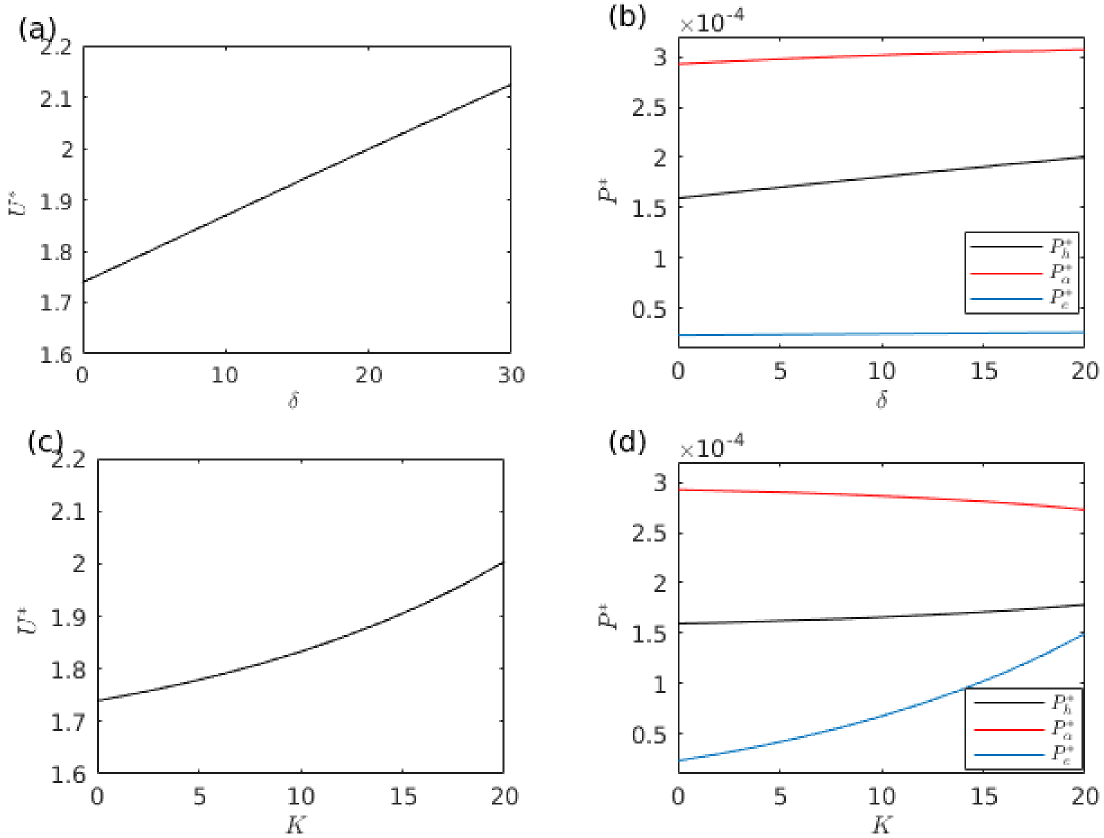

Figure 3.3: Flutter speed, average power per cycle at flutter speed dissipated by the plunge damper, dissipated by the pitch damper and at the load resistance as a function of nonlinear stiffness coefficent (a-b) and of nonlinear electromechanical coupling coefficient (c-d).

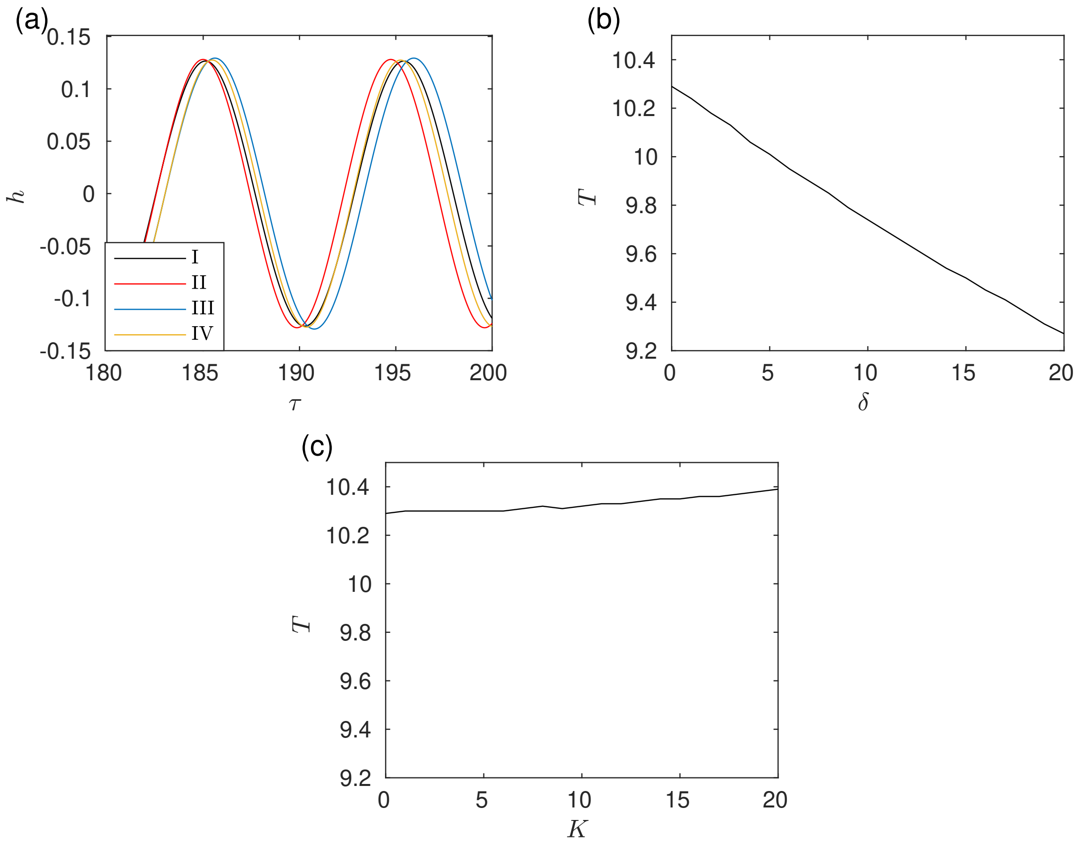

Figure 3.4: Plunge displacement as function of time for cases I–IV (a); period of oscillations as function of nonlinear stiffness coefficient (b) and of nonlinear piezoelectrical coupling coefficient (c).

Figure 3.5 shows projections of the state space in three planes, namely [h, h'], [α, α'] and [v, α'], indicating the limit-cycle behaviour and changes in amplitudes. In the detailed regions, by comparing cases I and II, it is possible to see that δ increases amplitude of h, h', α' and v, although it decreases amplitude of α. By comparing cases I and III, it is possible to see that K increases amplitude of h, h' and v, while it decreases amplitude of α and α'. It is interesting to note that the combined effect of δ and K at these values decrease h and h'. Overall, the mechanical variables of the system are more sensitive to δ, while v is more sensitive to K.

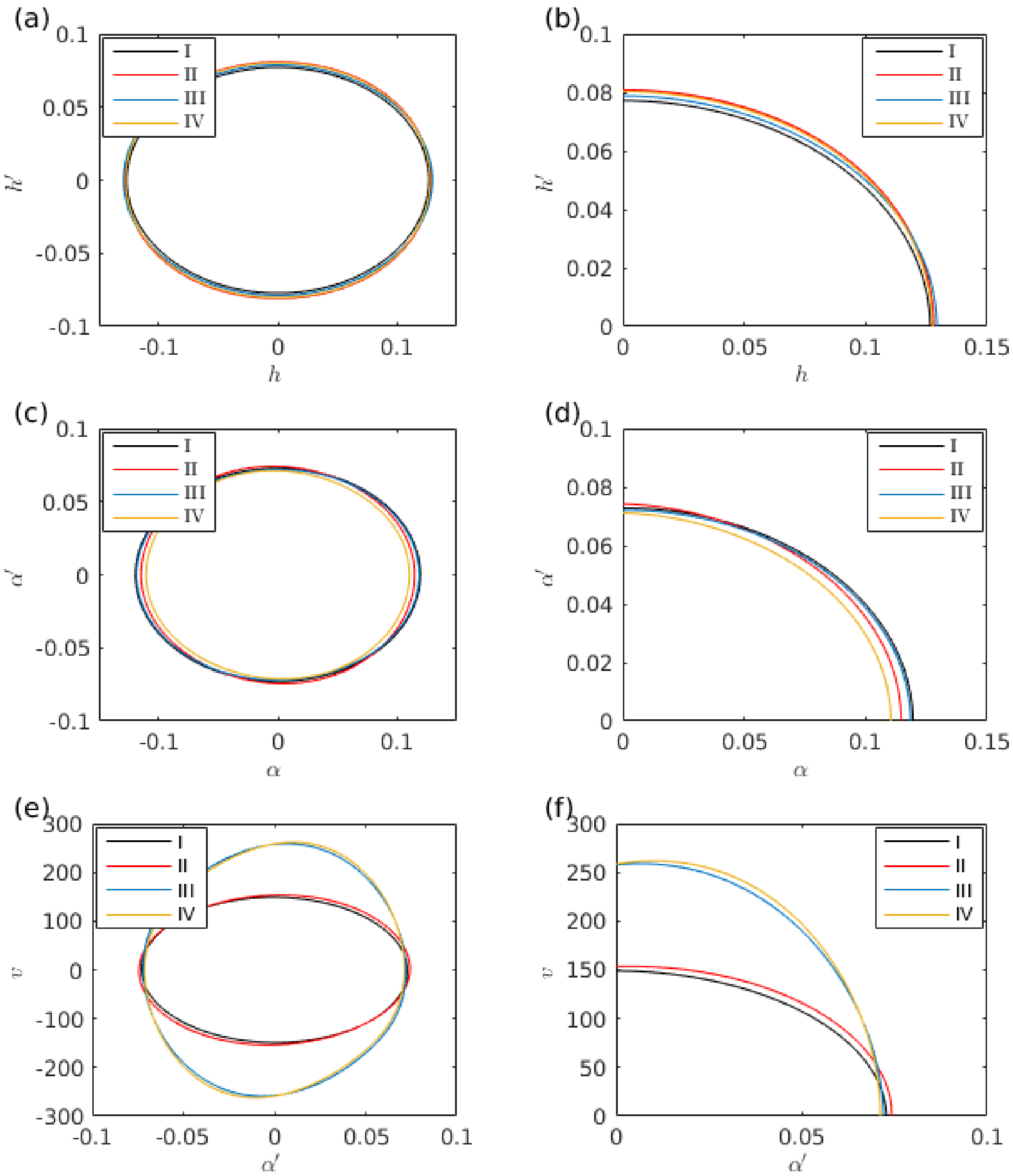

Figure 3.5: Projections of the state space in: (a) [h, h'] with detail in (b); (c) [α, α'] with detail in (d); (e) [v, α'] with detail in (f).

3.3 Mechanical and electrical power as a function of the wind speed

In this section, the mechanical and electrical power as a function of the wind speed is verified for case I, case II, case V and case VI. Table 3.3 shows flutter speed and average mechanical power related to plunge ($\bar{P}_h$), to pitch ($\bar{P}_\alpha$) and electrical power ($\bar{P}_e$) for cases I, II, V and VI, with $\kappa = 5 \times 10^{-6}$, $n = 3.66 \times 10^{-9}$, $\lambda = 0.48 \times 10^{9}$, This result indicates that piezoelectric transducer increases flutter speed. The use of nonlinear stiffness also increases the flutter speed.

Table 3.3: Flutter speed and Average Power per cycle for cases I–II and V–VI.

Cases	U^*	$\overline{P_h}$	$\overline{P_\alpha}$	$\overline{P_e}$
I	1.7247	1.586×10^{-4}	2.937×10^{-4}	1.654×10^{-5}
II	1.8446	1.671×10^{-4}	2.838×10^{-4}	1.648×10^{-5}
V	1.6915	1.975×10^{-4}	3.735×10^{-4}	–
VI	1.8112	1.774×10^{-4}	3.076×10^{-4}	–

Figures 3.6 and 3.7 shows the average power as a function of U. This result indicates that piezoelectric transducer decreases mechanical power. The use of nonlinear stiffness decreases electrical power collected from energy harvesting in 0.036%, for these parameters, what indicates that using nonlinear stiffness influence in the energy harvesting of the system presented.

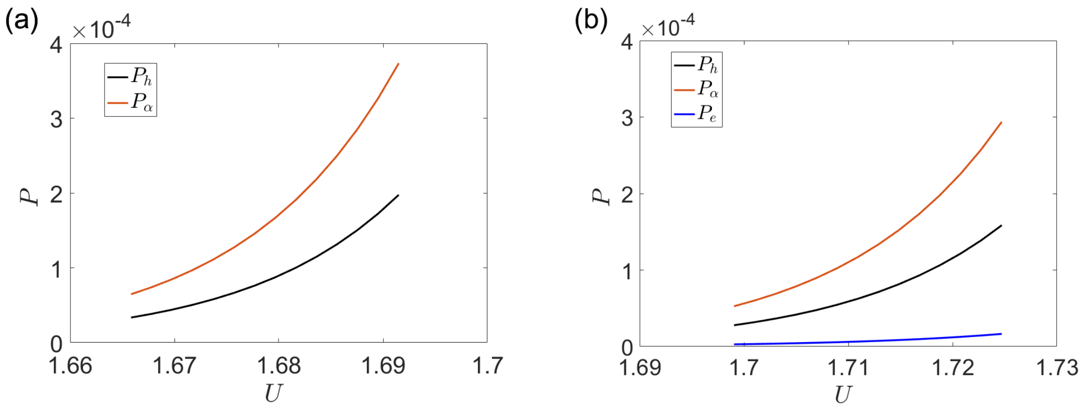

Figure 3.6: Average power as function of speed (U) for (a) case (V), (b) case (I).

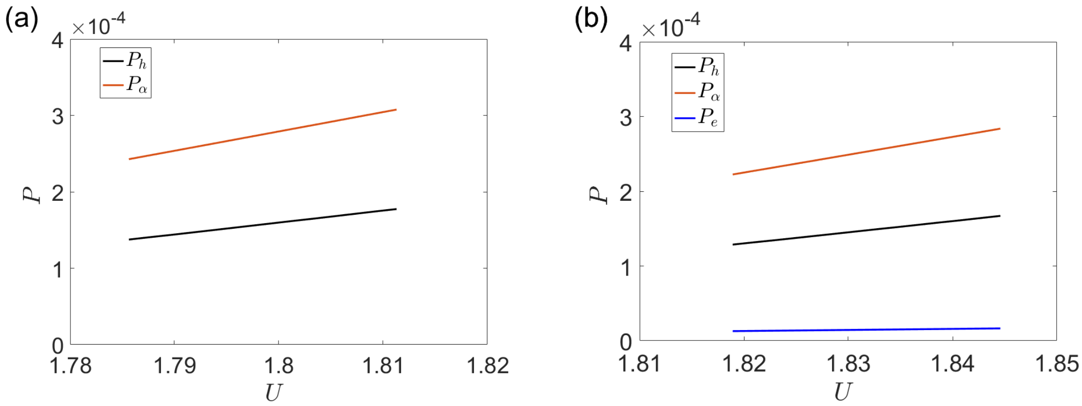

Figure 3.7: Average power as function of speed (U) for (a) case (VI), (b) case (II).

Chapter 4

System behaviour as function of electrical parameters

In this chapter, the flutter speed is analysed as function of the electrical parameters, specifically the electromechanical coupling (κ), the electrical resistance (λ), and the equivalent capacitance (η). Also, mechanical and electrical power, related to plunge, pitch and voltage degrees of freedom, are analysed as function of these parameters, to evaluate the influence of nonlinear stiffness and nonlinear electromechanical coupling in the dynamical behaviour of the aeroelastic system.

4.1 Flutter speed as a function of the electromechanical coupling

Flutter speed as a function of the electromechanical coupling is compared for four cases: case I, case II, case III, case IV. So the influence of the nonlinear stiffness ($\delta = 10$) and nonlinear electromechanical coupling ($K = 2$) is verified. The electromechanical coupling (κ) varies from 2×10^{-6} to 8×10^{-6}, $\lambda = 0.48 \times 10^{9}$ and $\eta = 3.66 \times 10^{-9}$.

Figure 4.1 shows variation of flutter speed as a function of electromechanical coupling for cases I–IV and table 4.1 gives the values of U^*, P_h^*, P_α^* and P_e^* for cases I–IV, with

$\kappa = 2.0 \times 10^{-6}$ and $\kappa = 8.0 \times 10^{-6}$..

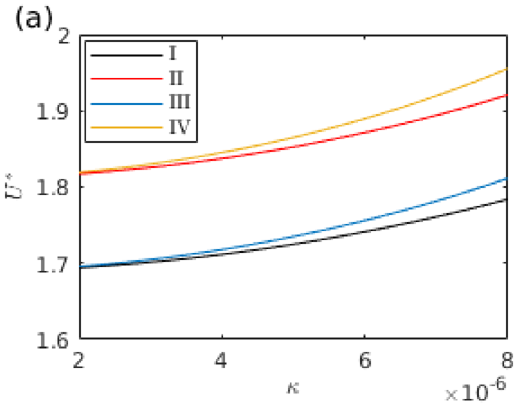

Figure 4.1: Flutter speed as a function of the electromechanical coupling for cases I–IV.

Table 4.1: Flutter speed and average power per cycle at flutter speed for cases I–IV, for $\kappa = 2 \times 10^{-6}$, $\kappa = 8 \times 10^{-6}$.

Case	U^* $\kappa = 2.0 \times 10^{-6}$	U^* $\kappa = 8 \times 10^{-6}$	$\overline{P}_e$ $\kappa = 2.0 \times 10^{-6}$	$\overline{P}_e$ $\kappa = 8 \times 10^{-6}$
I	1.694	1.784	2.616×10^{-6}	4.336×10^{-5}
II	1.817	1.921	2.784×10^{-6}	4.628×10^{-5}
III	1.696	1.811	3.342×10^{-6}	5.64×10^{-5}
IV	1.819	1.955	3.602×10^{-6}	6.11×10^{-5}

These results show that U^* increases with κ, and that the presence of either nonlinear stiffness or nonlinear coupling increase U^* for all values of κ in this range. The combination of both nonlinear terms (case IV) results in largest U^*, and the difference between all cases increases with κ. For example, at $\kappa = 8 \times 10{-}6$, there is an increase of $7,679\%$ in U^* when comparing case II to I, 1.51% when comparing case III to I, and of 9.59% when comparing IV to I. It is noted that δ has larger influence than K. Increasing flutter speed is interesting for aeronautics, because it can indicate that flight speed can be increased.

Figures 4.2, 4.3 and 4.4 show plunge displacement (h), pitch displacement (α), and electrical voltage (v) as function of time τ, with $\kappa = 3 \times 10^{-6}$ and $\kappa = 7 \times 10^{-6}$, for cases I – IV. Similar to U^*, the combination of both nonlinear terms (case IV) results in largest amplitude of h, but nonlinear stiffness increases more (case II), when compared to nonlinear electromechanical coupling (case III). The result is different for α, in which nonlinear stiffness and nonlinear electromechanical coupling decreases pitch displacement. However case III has very less influence in the displacement, when compared to case II. About v, nonlinear stiffness and nonlinear electromechanical coupling increases the amplitude, but case III has the highest influence in comparison to case II, and also the combination of both nonlinear terms (case IV) results in largest amplitude.

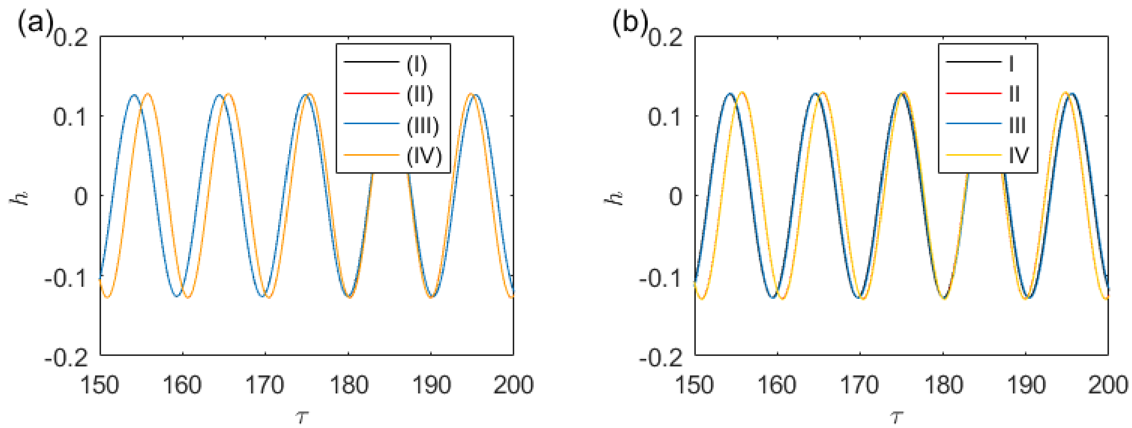

Figure 4.2: Plunge displacement as a function of time for cases (I)–(IV) (a) with $\kappa = 3 \times 10^{-6}$ and (b) with $\kappa = 7 \times 10^{-6}$.

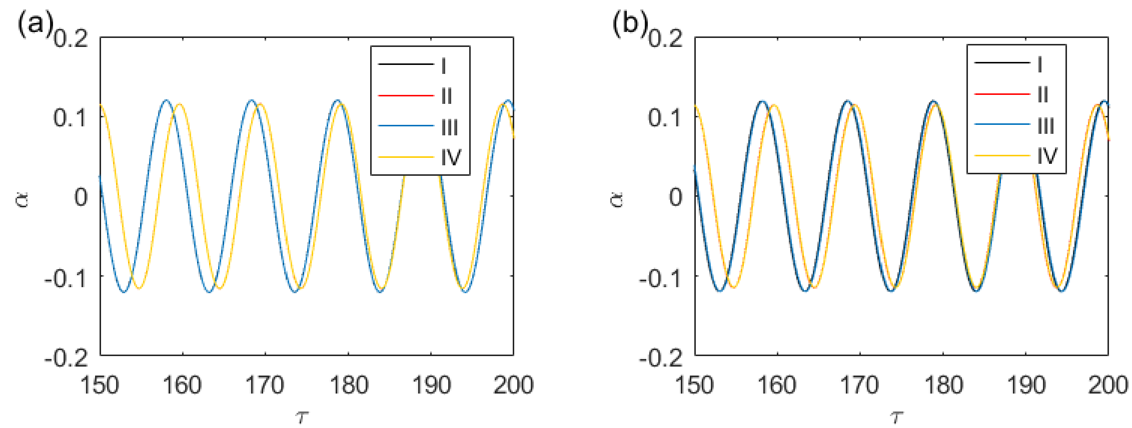

Figure 4.3: Pitch displacement as a function of time for cases (I)–(IV) (a) with $\kappa = 3 \times 10^{-6}$ and (b) with $\kappa = 7 \times 10^{-6}$.

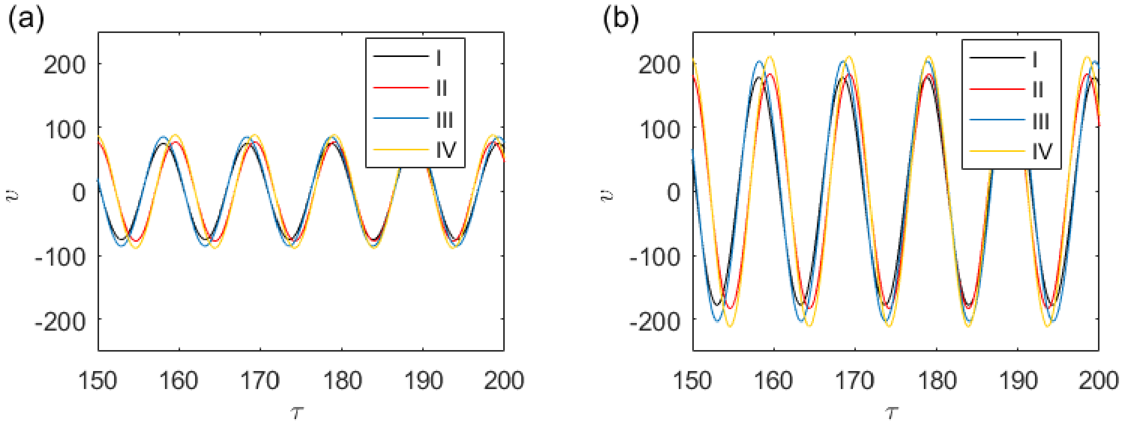

Figure 4.4: Electrical voltage as a function of time for cases (I)–(IV) (a) with $\kappa = 3\times10^{-6}$ and (b) with $\kappa = 7 \times 10^{-6}$.

4.1.1 Mechanical and electrical power as a function of the electromechanical coupling

Figure 4.5 shows variation of average electrical and mechanical power per cycle at flutter speed as a function of electromechanical coupling for cases I–IV.

Mechanical power related to plunge (P_h^*) increases for both δ and K, with largest values for case IV for all values of κ in this range, which is similar behaviour to U^*. Mechanical power related to pitch (P_α^*) has largest value for case II, as presence of nonlinear electromechanical coupling (cases III and IV) decreases (P_α^*) when compared to cases I and II, in which $K = 0$. The electrical power across the load resistance (P_e^*) increases with both nonlinear terms, similarly to U^* and P_h^*. However, K has larger influence than δ here, while still being larger when both nonlinear terms are present. For example, at $\kappa = 8 \times 10{-}6$, (P_e^*) increases by $6,07\%$ when comparing case II to I, by 30.07% when comparing case III to I, and by 40.91% when comparing IV to I.

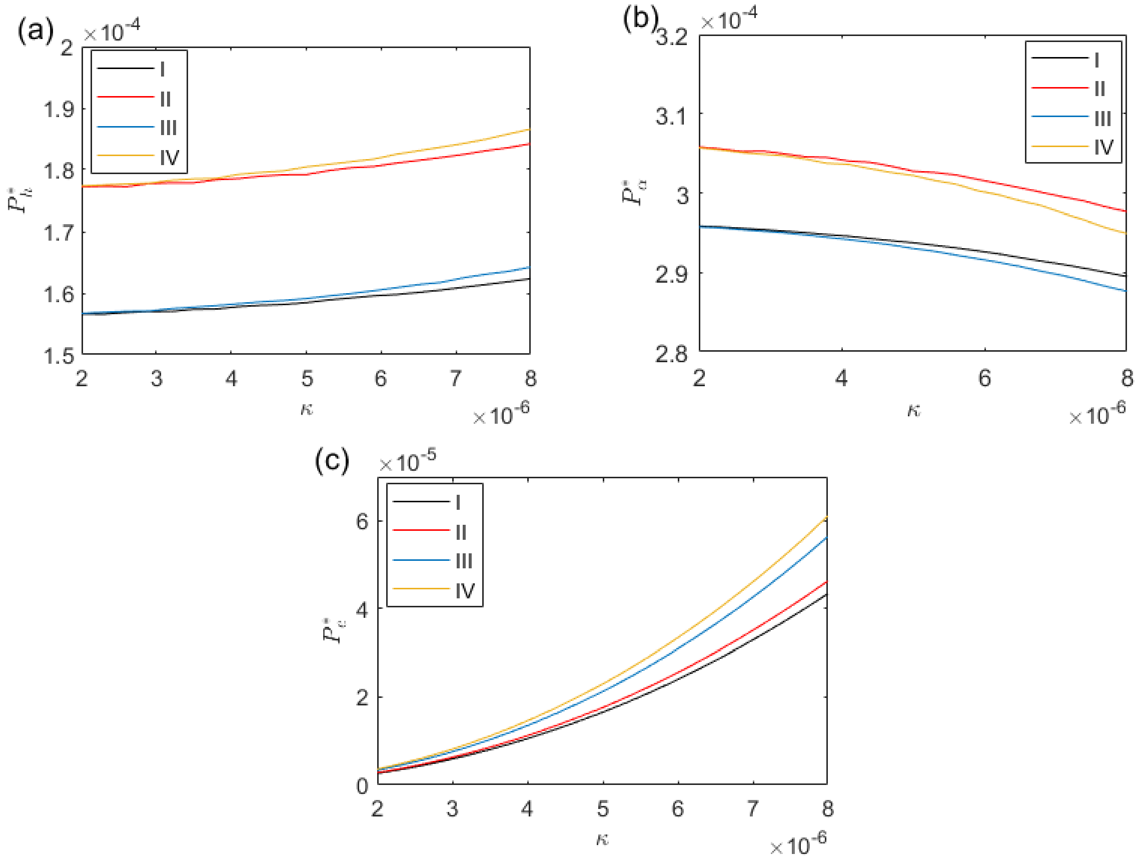

Figure 4.5: Power as a function of the electromechanical coupling for cases I–IV.

4.2 Flutter speed as a function of the electrical resistance

Flutter speed as a function of the electrical resistance is compared for four cases: case I, case II, case III, case IV. So the influence of the nonlinear stiffness ($\delta = 10$) and nonlinear electromechanical coupling ($K = 2$) is verified. The electrical resistance (λ) varies from 0.1×10^9 to 2×10^9, $\kappa = 5.9 \times 10^{-6}$ and $\eta = 3.66 \times 10^{-9}$.

Figure 4.6 shows variation of flutter speed as a function of the electrical resistance for cases I–IV.

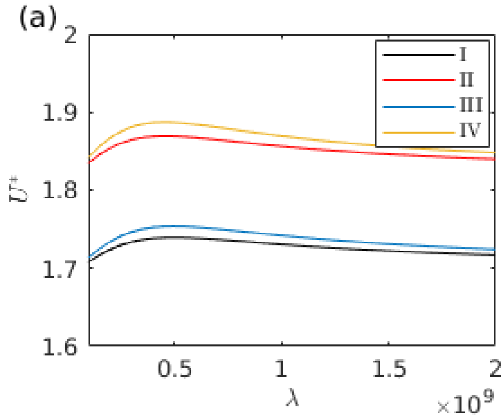

Figure 4.6: Flutter speed as a function of the electrical resistance for cases I–IV.

These results show that U^* has a maximum near $\lambda = 0.48 \times 10^9$, and the presence of both nonlinear terms increase U^* for all values of λ, with larger influence near the maximum. Again, it is noted that δ has larger influence than K.

Figures 4.7, 4.8 and 4.9 show plunge displacement (h), pitch displacement (α), and electrical voltage (v) as function of time τ, with $\lambda = 0.5 \times 10^9$ and $\lambda = 1.5 \times 10^9$, for cases I – IV. The results are the same as found for κ. h and v increases for case II and case III, but both nonlinear elements combined (case IV) causes the largest variation in amplitude. α decreases in all cases, and, again, causes IV causes the largest variation in amplitude. Nonlinear stiffness (δ) has the largest influence for h and α, and nonlinear electromechanical coupling (K) has the largest influence for v.

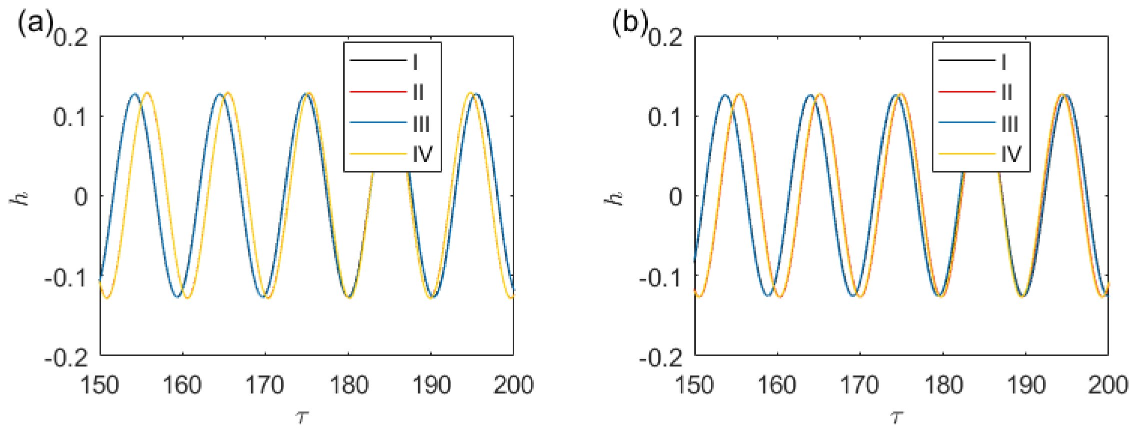

Figure 4.7: Plunge displacement as a function of time for cases (I)–(IV) (a) with $\lambda = 0.5 \times 10^9$ and (b) with $\lambda = 1.5 \times 10^9$.

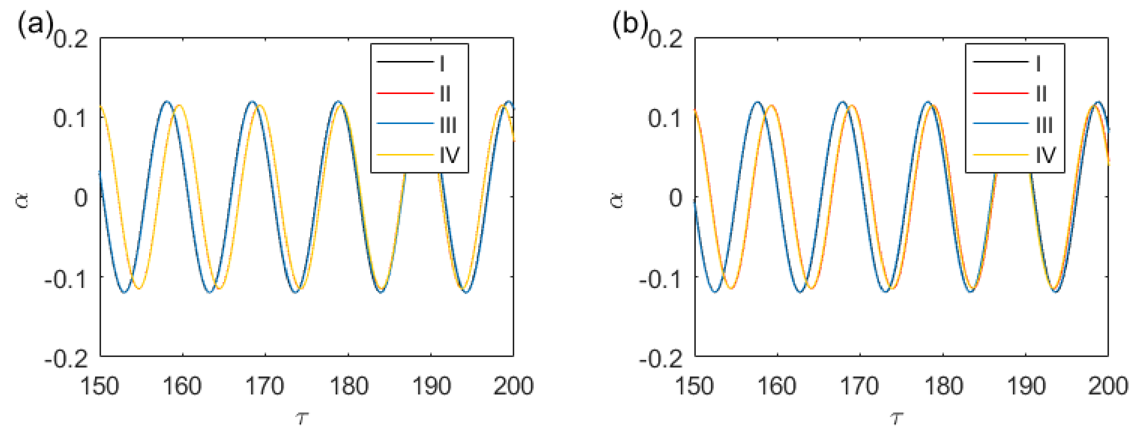

Figure 4.8: Pitch displacement as a function of time for cases (I)–(IV) (a) with $\lambda = 0.5 \times 10^9$ and (b) with $\lambda = 1.5 \times 10^9$.

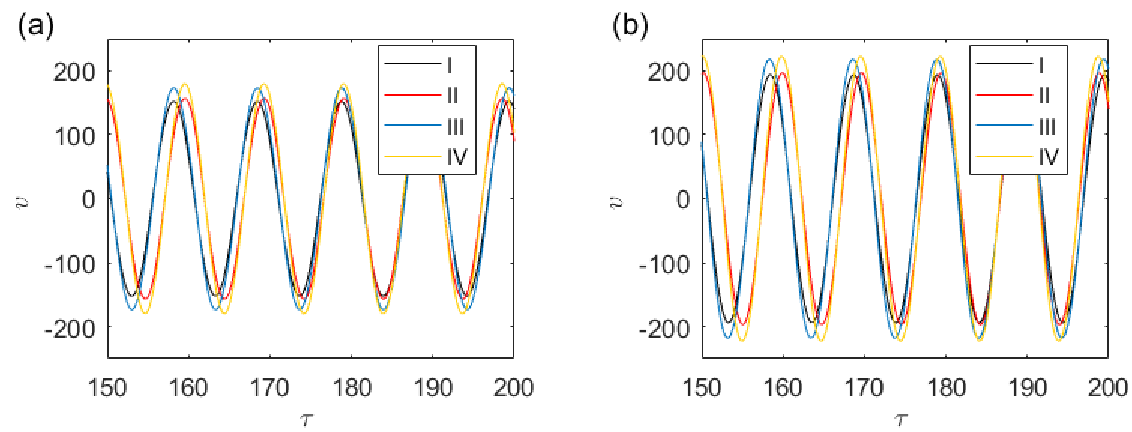

Figure 4.9: Electrical voltage as a function of time for cases (I)–(IV) (a) with $\lambda = 0.5 \times 10^9$ and (b) with $\lambda = 1.5 \times 10^9$.

4.2.1 Mechanical and electrical power as a function of the electrical resistance

Figure 4.10 shows variation of average electrical and mechanical power per cycle as a function of electrical resistance for cases I–IV.

Similarly to U^*, P_h^* and P_e^* increase with both nonlinear terms, although K has less influence at higher λ. Presence of K diminishes P_α^* , which is larger for case II, and insensitive to λ.

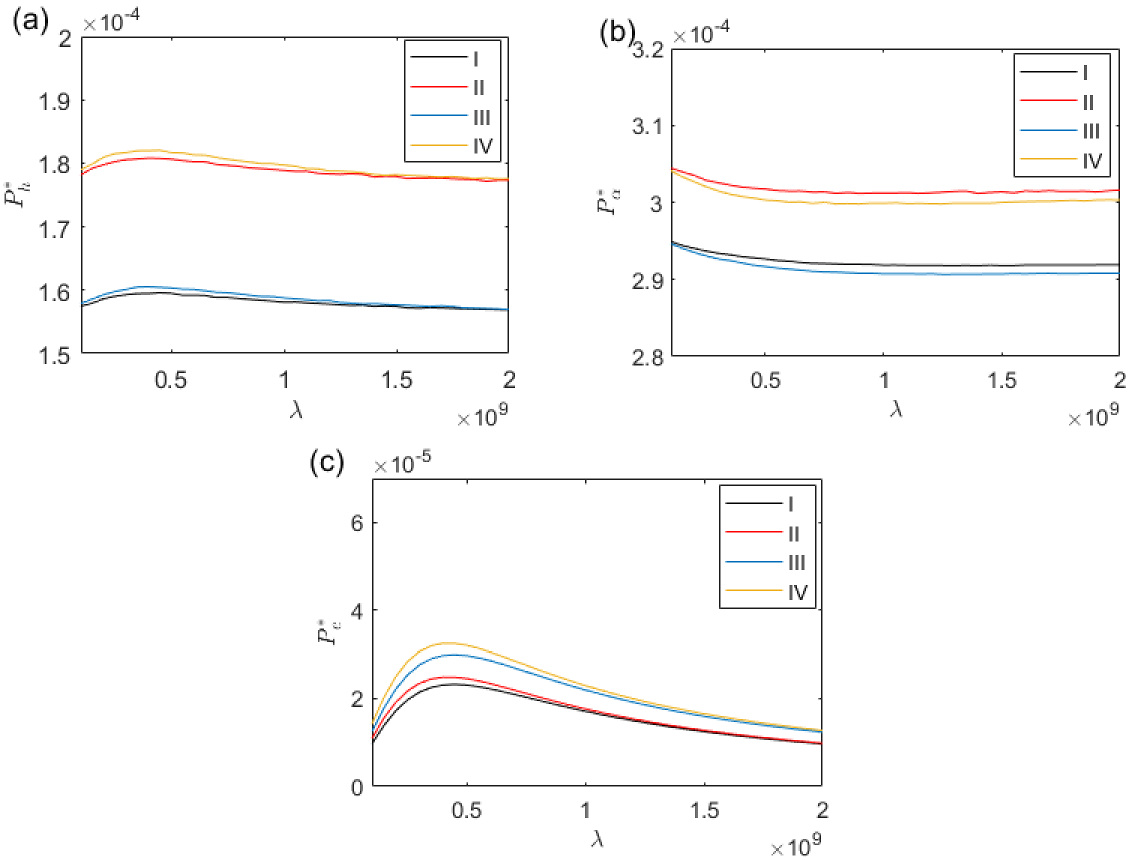

Figure 4.10: Power as a function of the electrical resistance for cases I–IV.

4.3 Flutter speed as a function of the equivalent capacitance

Flutter speed as a function of the equivalent capacitance is compared for four cases: case I, case II, case III, case IV. So the influence of the nonlinear stiffness ($\delta = 10$) and nonlinear electromechanical coupling ($K = 2$) is verified. The equivalent capacitance (η) varies from 2×10^{-9} to 5×10^{-9}, $\kappa = 5.9 \times 10^{-6}$ and $\lambda = 0.48 \times 10^{9}$.

Figure 4.11 shows variation of flutter speed as a function of the equivalent capacitance for cases I–IV.

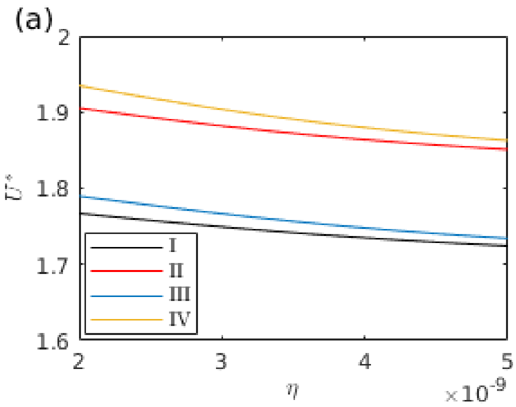

Figure 4.11: Flutter speed as a function of the equivalent capacitance for cases I–IV.

These results show that U^* decrease with η, while having largest values when both nonlinear terms are present (case IV).

Figures 4.12, 4.13 and 4.14 show plunge displacement (h), pitch displacement (α), and electrical voltage (v) as function of time τ, with $\eta = 2.5 \times 10^{-9}$ and $\eta = 4.5 \times 10^{-9}$, for cases I – IV. The results are the same as found for κ and λ. The results indicate that case IV has the highest influence in all displacements. For h, and v, an increase occurs, while for α, a decrease occurs. Again, δ has the largest influence for h and α, and K has the largest influence for v.

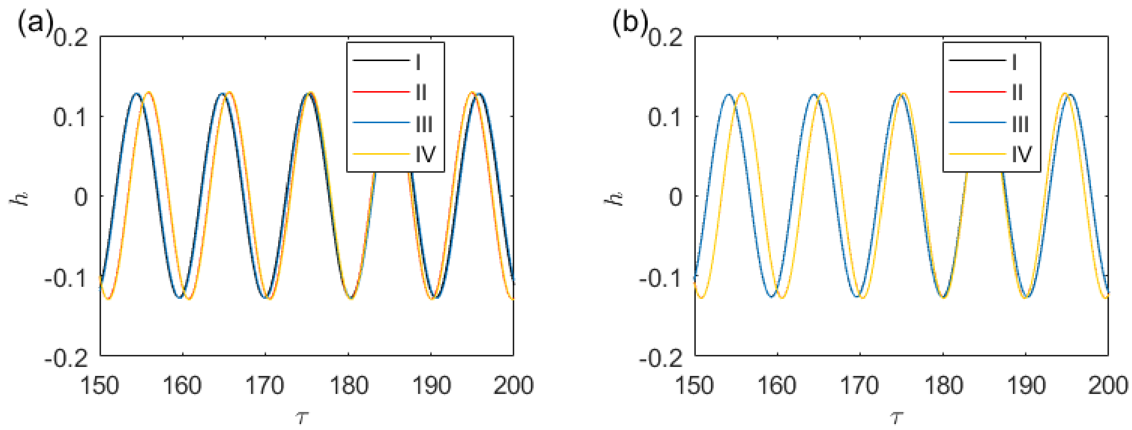

Figure 4.12: Plunge displacement as a function of time for cases (I)–(IV) (a) with $\eta = 2.5 \times 10^{-9}$ and (b) with $\eta = 4.5 \times 10^{-9}$.

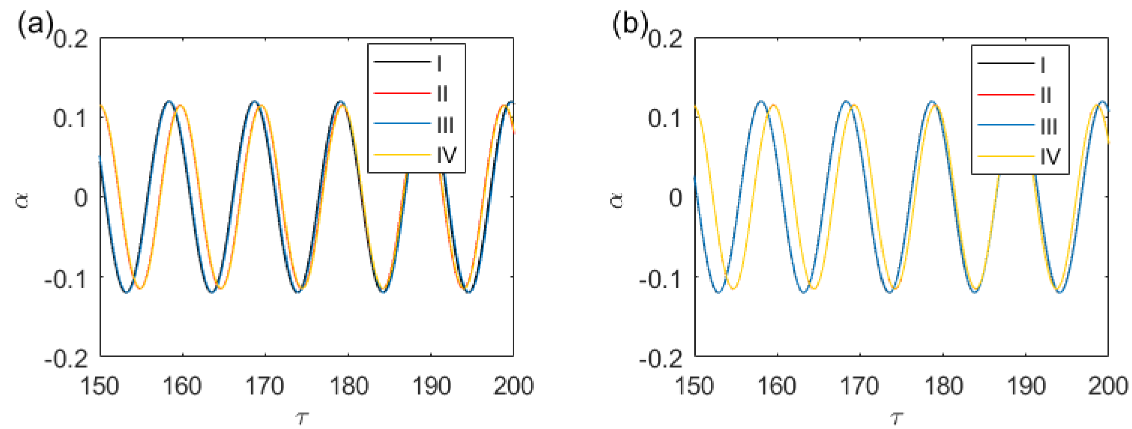

Figure 4.13: Pitch displacement as a function of time for cases (I)–(IV) (a) with $\eta = 2.5 \times 10^{-9}$ and (b) with $\eta = 4.5 \times 10^{-9}$.

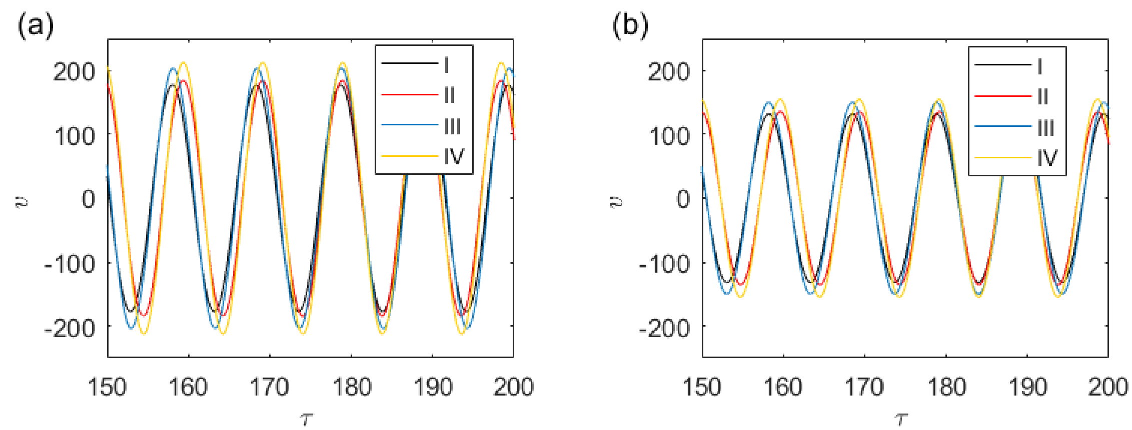

Figure 4.14: Electrical voltage as a function of time for cases (I)–(IV) (a) with $\eta = 2.5 \times 10^{-9}$ and (b) with $\eta = 4.5 \times 10^{-9}$.

4.3.1 Mechanical and electrical power as a function of the equivalent capacitance

Figure 4.15 shows variation of average electrical and mechanical power per cycle as a function of equivalent capacitance for cases I–IV.

Similarly to U^*, P_h^* and P_e^* decrease with η, and have the largest values for case IV. Similarly to the previous results, P_e^* shows more sensitivity to K than to δ, as can be observed by comparing cases II and III. P_α^* increases with η, and again has larger value for case II. All four quantities become less sensitive as η increases.

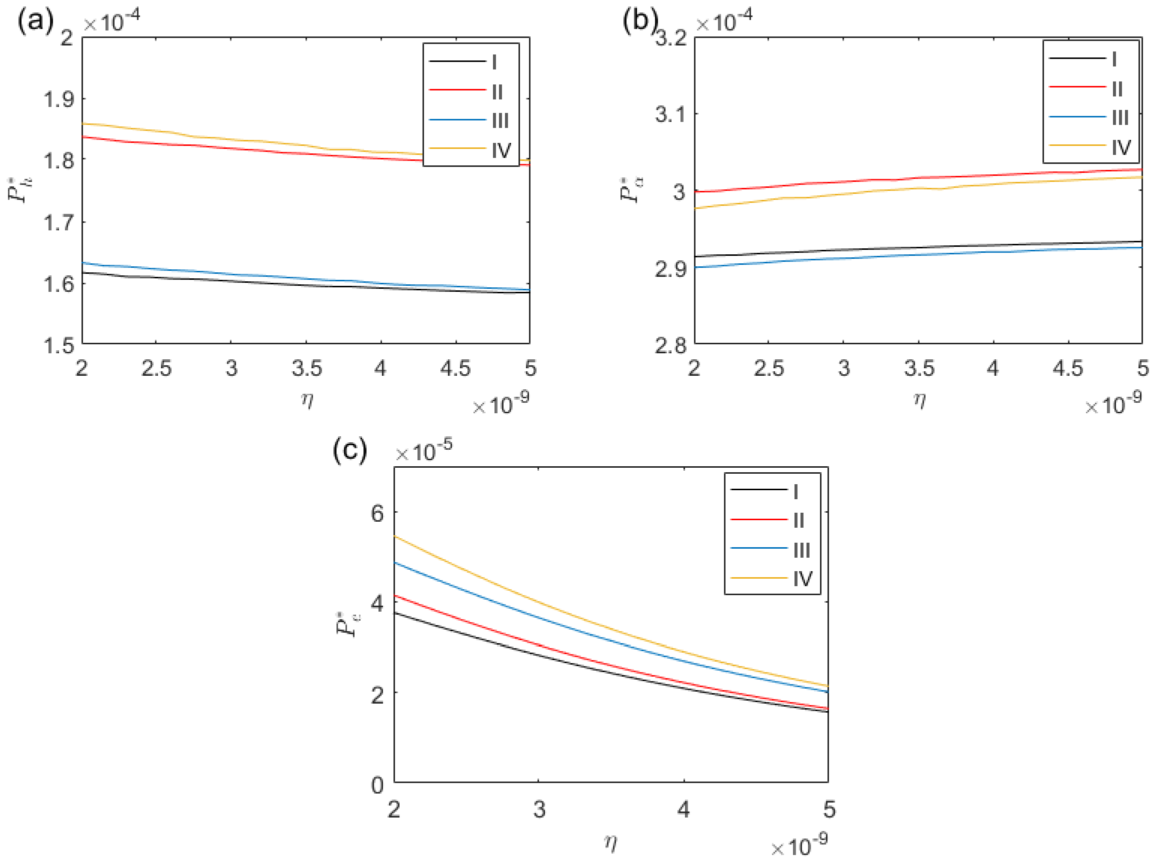

Figure 4.15: Power as a function of the equivalent capacitance for cases I–IV.

4.4 Flutter speed and electrical power surface as a function of two electrical parameters

Figure 4.16 summarises the results of this section for U^* and P_e^* for cases I–IV. It shows variation of U^* and P_e^* as a function of electromechanical coupling (κ) and electrical resistance (λ), and variation of U^* and P_e^* as a function of electromechanical coupling (κ) and equivalent capacitance (η). These results help to visualize the best combination of parameters to found the highest flutter speed and electrical power.

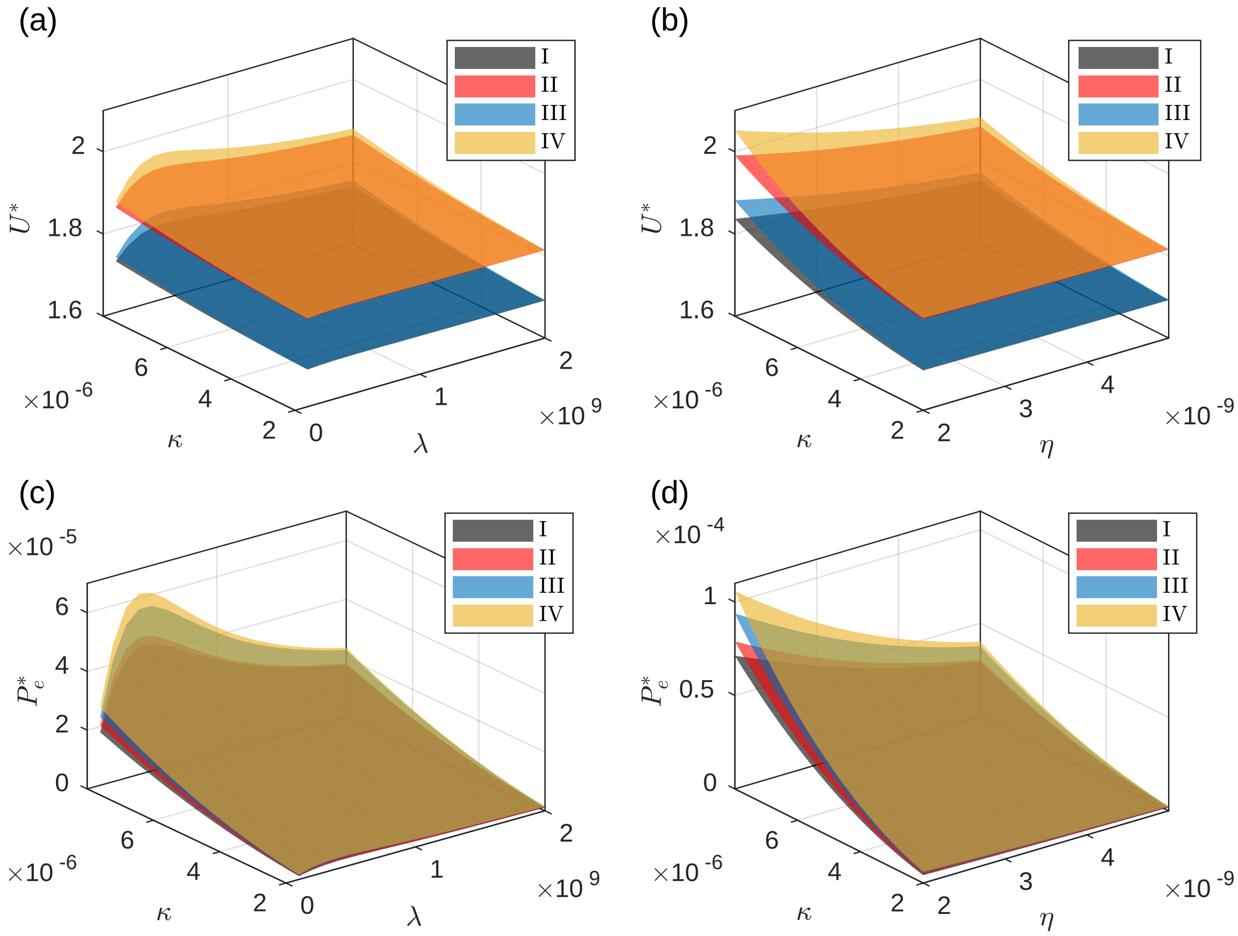

Figure 4.16: Flutter speed (a-b) and electrical power at the load resistance per cycle at flutter speed (c-d) as a function of electromechanical coupling, equivalent capacitance and electrical resistance for cases I–IV.

Tables 4.2 and 4.3 gives the values of U^*, P_h^*, P_α^* and P_e^* at the nominal parameters for cases I–IV with $\kappa = 3.0 \times 10^{-6}$ and $\kappa = 5.9 \times 10^{-6}$.

At $\kappa = 3 \times 10^{-6}$ and taking case I as baseline for comparisons, U^* increases by 7.324% in case II, by 0.206% in case III and by $7,559$% in case IV. P_e^* increases by 6.715% in case II, by 27.879% in case III and by 37.918% in case IV. At $\kappa = 5.9 \times 10^{-6}$, U^* increases by 7.497% in case II, by 0.822% in case III and by 8.469% in case IV. P_e^* increases by 6.828% in case II, by 28.800% in case III and by 38.917% in case IV. This shows that U^* is more sensitive to δ, while P_e^* is more sensitive to K. It is also interesting to note that the combined nonlinear terms have larger effect than when only one of them is present. For example, at $\kappa = 3 \times 10^{-6}$, P_e^* increases by 29.239% from case II to IV, and at $\kappa = 5.9 \times 10^{-6}$, P_e^* increases by 30.038% from case II to IV, meaning that nonlinear coupling increases P_e^* more when in presence of nonlinear stiffness than otherwise, indicated by comparing case III and I. Similarly, P_e^* increases by 7.850%, at $\kappa = 3 \times 10^{-6}$, and by 7.854%, at $\kappa = 5.9 \times 10^{-6}$, from case III to IV, meaning that nonlinear stiffness increases P_e^* more when in presence of nonlinear coupling than otherwise, indicated by comparing case II and I. Therefore, the presence of one nolinear term enhances the effect of the other, what makes the case IV the most interesting one to rise flutter speed and electrical power.

Table 4.2: Flutter speed and average power per cycle at flutter speed for cases I–IV, with $\kappa = 3 \times 10{-}6$.

Case	U^*	P_h^* $\times 10^{-4}$	P_α^* $\times 10^{-4}$	P_e^* $\times 10^{-5}$
I	1.7012	1.5691	2.9534	0.5897
II	1.8258	1.7785	3.0554	0.6293
III	1.7047	1.5709	2.9500	0.7541
IV	1.8298	1.7764	3.0441	0.8133

Table 4.3: Flutter speed and average power per cycle at flutter speed for cases I–IV, with $\kappa = 5.9 \times 10{-}6$.

Case	U^*	P_h^* $\times 10^{-4}$	P_α^* $\times 10^{-4}$	P_e^* $\times 10^{-5}$
I	1.7393	1.5939	2.9270	2.3170
II	1.8697	1.8108	3.0240	2.4752
III	1.7536	1.6035	2.9168	2.9843
IV	1.8866	1.8132	2.9971	3.2187

Chapter 5

Conclusions

In this work, the dynamic behaviour of an aeroelastic energy harvesting system using a piezoelectric transducer was studied, considering nonlinear stiffness and nonlinear electromechanical coupling. The main cases showed the behaviour of a linear system, the effect of each nonlinear term separately, and the combined effect of both nonlinear terms. The aerodynamic models of Edwards (1979) and Dimitriadis (2017) were compared: the major difference between the results using these two models is at lower values of κ.

The results for the analysed system indicate that nonlinear stiffness has more influence in increasing flutter speed, and nonlinear piezoelectric coupling has more influence in increasing electrical power, however the best scenario is given by the combined nonlinear elements.

These results provide evidence that, by increasing the electromechanical coupling, either through the linear or nonlinear term, more energy is transferred from the mechanical domain to the electrical domain, which is expected and contributes to the resulting increase in flutter speed, but also that more energy is transferred from the pitch motion than from the plunge motion, as shown by the behaviour of α and P^*_α, which both decrease with κ (linear) and K (nonlinear). Specifically, increasing the nonlinear term causes a decrease of P^*_α in all analysed situations and parameter values. Flutter speed, mechanical and electrical power increase with δ, indicating that neglecting the nonlinear stiffness characteristic can lead to underestimation of flutter speed and harvested energy.

Increasing the amount of energy harvested using combined nonlinear elements has the potential to increase the applicability of energy harvesting to aeronautical structures and engineering systems in general. Further analysis can be performed to better understand this energy transfer characteristic using concepts of Targeted Energy Tranfer and Nonlinear Normal Modes.

Chapter 6

Publications

6.1 Publications

1. A. C. G. Amaral and M. Silveira, Aplicação de energy harvesting piezoelétrico em estruturas aeronáuticas em condição de flutter. In: XI Seminário da pós graduação em engenharia mecânica, 2018, Bauru, São Paulo.

2. A. C. G. Amaral and M. Silveira, Dissipated energy analysis of aeroelastic system with nonlinear stiffness, with application to energy harvesting. In: 25 International Congress of Mechanical Engineerring, COBEM 2019, Uberlândia, Minas Gerais.

3. A. C. G. Amaral and M. Silveira, Dissipated energy analysis of aeroelastic system with nonlinear stiffness, with application to energy harvesting. In: XII Seminário da pós graduação em engenharia mecânica, 2019, Bauru, São Paulo.

Bibliography

A. Abdelkefi, M. R. Hajj, and A. H. Nayfeh. Piezoelectric energy harvesting from transverse galloping of bluff bodies. *Smart Materials and Structures*, 22(1):015014, 2012a.

A. Abdelkefi, A. H. Nayfeh, and M. R. Hajj. Modeling and analysis of piezoaeroelastic energy harvesters. *Nonlinear Dynamics*, 67(2):925–939, 2012b.

R. Amirtharajah and A. P. Chandrakasan. Self-powered signal processing using vibration-based power generation. *IEEE Journal of Solid-state Circuits*, 33(5):687–695, 1998.

A. Bibo and M. F. Daqaq. Energy harvesting under combined aerodynamic and base excitations. *Journal of Sound and Vibration*, 332(20):5086–5102, 2013.

R. L. Bisplinghoff, H. Ashley, and R. L. Halfman. *Aeroelasticity*. Courier Corporation, 2013.

R. Caliò, U. B. Rongala, D. Camboni, M. Milazzo, C. Stefanini, G. Petris, and C. M. Oddo. Piezoelectric energy harvesting solutions. *Sensors*, 14(3):4755–4790, 2014.

A. R. Collar. The expanding domain of aeroelasticity. *The Aeronautical Journal*, 50 (428):613–636, 1946.

E. F. Crawley and E. H. Anderson. Detailed models of piezoceramic actuation of beams. *Journal of Intelligent Material Systems and Structures*, 1(1):4–25, 1990.

M. F. Daqaq, R. Masana, A. Erturk, and D. D. Quinn. On the role of nonlinearities in vibratory energy harvesting: a critical review and discussion. *Applied Mechanics Reviews*, 66(4), 2014.

G. Dimitriadis. *Introduction to Nonlinear Aeroelasticity*, volume 1. John Wiley & Sons, 2017.

N. E. DuToit and B. L. Wardle. Experimental verification of models for microfabricated piezoelectric vibration energy harvesters. *AIAA Journal*, 45(5):1126–1137, 2007.

J. W. Edwards. Unsteady aerodynamic modeling for arbitrary motions. *The American Institute of Aeronautics and Astronautics*, 17:365–374, 1979.

M. Ericka, D. Vasic, F. Costa, G. Poulin, and S. Tliba. Energy harvesting from vibration using a piezoelectric membrane. In *Journal de Physique IV (Proceedings)*, volume 128, pages 187–193. EDP sciences, 2005.

A. Erturk, J. Hoffmann, and D. J. Inman. A piezomagnetoelastic structure for broadband vibration energy harvesting. *Applied Physics Letters*, 94(25):254102, 2009.

A. Erturk, W. G. R. Vieira, C. Marqui Jr, and D. J. Inman. On the energy harvesting potential of piezoaeroelastic systems. *Applied Physics Letters*, 96(18):184103, 2010.

G. Gatti, M. J. Brennan, M. G. Tehrani, and D. J. Thompson. Harvesting energy from the vibration of a passing train using a single-degree-of-freedom oscillator. *Mechanical Systems and Signal Processing*, 66-67:785–792, 2016.

F. Goldschmidtboeing, C. Eichhorn, M. Wischke, M. Kroener, and P. Woias. The influence of ferroelastic hysteresis on mechanically excited pzt cantilever beams. In *Proceedings of the 11th International Workshop on Micro and Nanotechnology for Power Generation and Energy Conversion Applications*, pages 114–117, 2011.

A. Harb. Energy harvesting: State-of-the-art. *Renewable Energy*, 36:2641–2654, 2011.

Y. Hu, H. Xue, J. Yang, and Q. Jiang. Nonlinear behavior of a piezoelectric power harvester near resonance. *IEEE Transactions on Ultrasonics, Ferroelectrics, and Frequency Control*, 53(7):1387–1391, 2006.

E. Jonsson, C. Riso, C. A. Lupp, C. E. S. Cesnik, J. Martins, and B. I. Epureanu. Flutter and post-flutter constraints in aircraft design optimization. *Progress in Aerospace Sciences*, 2019.

H. Jung and S. Lee. The experimental validation of a new energy harvesting system based on the wake galloping phenomenon. *Smart Materials and Structures*, 20(5): 055022, 2011.

M. G. Kang, W. S. Jung, C. Y. Kang, and S. J. Yoon. Recent progress on pzt based piezoelectric energy harvesting technologies. In *Actuators*, volume 5, page 5. Multidisciplinary Digital Publishing Institute, 2016.

S. Leadenham and A. Erturk. Unified nonlinear electroelastic dynamics of a bimorph piezoelectric cantilever for energy harvesting, sensing, and actuation. *Nonlinear Dynamics*, 79(3):1727–1743, 2015.

C. Marqui Jr and A. Erturk. Electroaeroelastic analysis of airfoil-based wind energy harvesting using piezoelectric transduction and electromagnetic induction. *Journal of Intelligent Material Systems and Structures*, 24:846–854, 2013.

C. Marqui Jr, D. Tan, and A. Erturk. On the electrode segmentation for piezoelectric energy harvesting from nonlinear limit cycle oscillations in axial flow. *Journal of Fluids and Structures*, 82:492–504, 2018.

E. M. Marqui Jr, C. Belo and F. D. Marques. A flutter suppression active controller. *Proceedings of the Institution of Mechanical Engineers, Part G: Journal of Aerospace Engineering*, 219(1):19–33, 2005.

F. I. Petrescu, A. Apicella, R. V. Petrescu, S. Kozaitis, R. Bucinell, R. Aversa, and T. Abu-Lebdeh. Environmental protection through nuclear energy. *American Journal of Applied Sciences*, 13(9):941–946, 2016.

S. Roundy and P. K. Wright. A piezoelectric vibration based generator for wireless electronics. *Smart Materials and structures*, 13(5):1131, 2004.

M. Safaei, H. A. Sodano, and S. R. Anton. A review of energy harvesting using piezoelectric materials: state-of-the-art a decade later (2008–2018). *Smart Materials and Structures*, 28(11):113001, 2019.

V. C. Sousa, M. de M Anicézio, C. De Marqui Jr, and A. Erturk. Enhanced aeroelastic energy harvesting by exploiting combined nonlinearities: theory and experiment. *Smart Materials and Structure*, 20:094007, 2011.

V. C. Sousa, T. M. P. Silva, and C. Marqui Jr. Aeroelastic flutter enhancement by exploiting the combined use of shape memory alloys and nonlinear piezoelectric circuits. *Journal of Sound and Vibration*, 407:46–62, 2017.

N. G. Stephen. On energy harvesting from ambient vibration. *Journal of Sound and Vibration*, 293(1-2):409–425, 2006.

D. Tan, P. Yavarow, and A. Erturk. Nonlinear elastodynamics of piezoelectric macro-fiber composites with interdigitated electrodes for resonant actuation. *Composite Structures*, 187:137–143, 2018a.

D. Tan, P. Yavarow, and A. Erturk. Resonant nonlinearities of piezoelectric macro-fiber composite cantilevers with interdigitated electrodes in energy harvesting. *Nonlinear Dynamics*, 92(4):1935–1945, 2018b.

D. Tang and E. H. Dowell. Flutter and limit-cycle oscillations for a wing-store model with freeplay. *Journal of Aircraft*, 43(2):487–503, 2006.

L. Tang, M. P. Païdoussis, and J. Jiang. Cantilevered flexible plates in axial flow: energy transfer and the concept of flutter-mill. *Journal of Sound and Vibration*, 326(1-2): 263–276, 2009.

M. G. Tehrani and S. J. Elliott. Extending the dynamic range of an energy harvester using nonlinear damping. *Journal of Sound and Vibration*, 333:623–629, 2014.

A. Triplett and D. D. Quinn. The effect of non-linear piezoelectric coupling on vibration-based energy harvesting. *Journal of Intelligent Material Systems and Structures*, 20 (16):1959–1967, 2009.

W. H. Tsai, Y. C. Chang, S. J. Lin, H. C. Chen, and P. Y. Chu. A green approach to the weight reduction of aircraft cabins. *Journal of Air Transport Management*, 40: 65–77, 2014.

N. Tsushima and W. Su. Flutter suppression for highly flexible wings using passive and active piezoelectric effects. *Aerospace Science and Technology*, 65:78–89, 2017.

W. Wang, J. Cao, C. R. Bowen, S. Zhou, and J. Lin. Optimum resistance analysis and experimental verification of nonlinear piezoelectric energy harvesting from human motions. *Energy*, 118:221–230, 2017.

Z. Wang, X. Xu, Y. Zhu, and T. Gan. Evaluation of carbon emission efficiency in china's airlines. *Journal of Cleaner Production*, 243:118500, 2020.

C. Wei and X. Jing. A comprehensive review on vibration energy harvesting: Modelling and realization. *Renewable and Sustainable Energy Reviews*, 74:1–18, 2017.

Z. Yang, A. Erturk, and J. Zu. On the efficiency of piezoelectric energy harvesters. *Extreme Mechanics Letters*, 15:26–37, 2017.

N. Yoon, C. Chung, Y. H. Na, and S. Shin. Control reversal and torsional divergence analysis for a high-aspect-ratio wing. *Journal of Mechanical Science and Technology*, 26(12):3921–3931, 2012.

L. B. Zhang, A. Abdelkefi, H. L. Dai, R. Naseer, and L. Wang. Design and experimental analysis of broadband energy harvesting from vortex-induced vibrations. *Journal of Sound and Vibration*, 408:210–219, 2017a.

Y. Zhang, K. Guo, D. Wang, C. Chen, and X. Li. Energy conversion mechanism and regenerative potential of vehicle suspensions. *Energy*, 119:961–970, 2017b.

L. Zuo, B. Scully, J. Shestani, and Y. Zhou. Design and characterization of an electromagnetic energy harvester for vehicle suspensions. *Smart Materials and Structures*, 19(4):045003, 2010.